Chapter-6

Tribological studies of chemically modified biolubricants and their admixture with different nano-additives

This chapter explains the chemical modification of the biolubricants to reduce its unsaturation. The process opted for the modification was epoxidation. In this process, the active sites (C=C) for the different undesired reaction was altered with the epoxy group. Thereafter, the epoxidized biolubricants tested with different types of additives to examine the tribo-performance.

6.1. Modification of biolubricants by epoxidation method

6.1.1. Epoxidation of rapeseed oil, sunflower and castor oil

The structure of the fatty acid chain was altered by the epoxidation method for the explored biolubricants. The main purpose of this process to remove the C=C from the fatty acid chain. The similar procedure was applicable for each vegetable oil with only difference in reactant molar ratio. The same molar ratio (oil: formic acid: hydrogen peroxide) was used for rapeseed oil (RO) and sunflower oil (SO) and it was 1:2:20. While for castor oil (CO) this molar ratio was 1:0.5:1.5 and acetic acid used in place of formic acid. In the epoxidation process both formic and acetic acid perform as an oxygen carrier, while hydrogen peroxide used as the oxygen donor. H_2SO_4 was also used in a small quantity to act as catalyst to boost the reaction rate. Epoxidation experimental set-up is presented in Figure 6.1. One of the inclined necks of three-necked round flask was used to pour the measured amount of

biolubricant, while thermometer was inserted via other inclined neck. At first, biolubricant and formic/acetic acid simultaneously heated and stirred at 65ºC and 600 rpm respectively. Subsequently, H_2SO_4 (2 ml) was added in the heated solution. Thereafter measured quantity of hydrogen peroxide mixed for 30 minutes drop-wise in the heated solution. As the hydrogen peroxide added, the solution temperature suddenly shoots up due to exothermic reaction. Therefore ice or chilled water was used to maintain the solution temperature to 65ºC. Also, the evaporated solution was liquefied using water jacketed reflux condenser. The reaction was completed in 6 hours (approximately). After completion of the epoxidation reaction, the solution was instantly extracted with diethyl ether. Thereafter deionized water was used to wash and remove free fatty acid, if any.

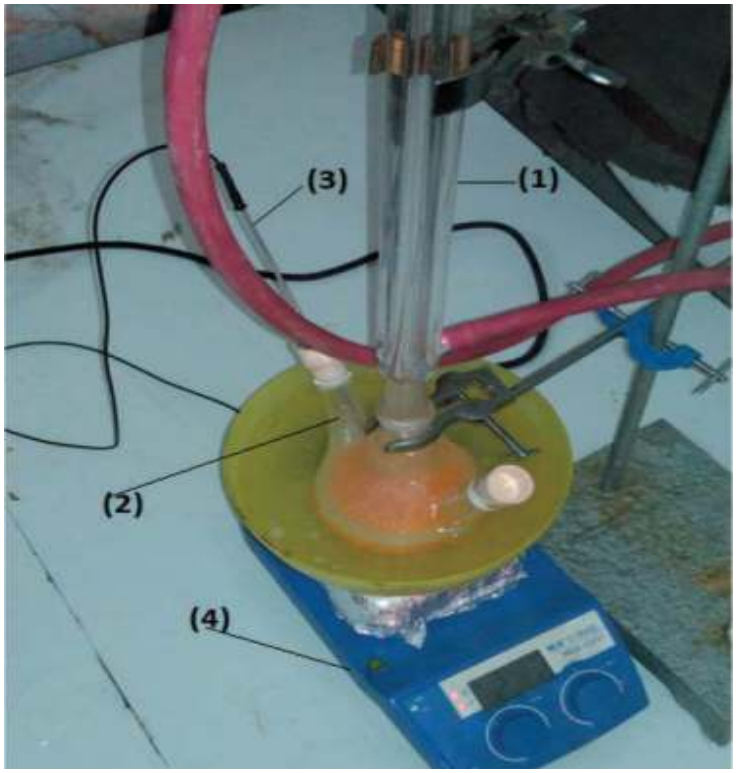

Figure 6.1. Typical experimental set-up for epoxidation consist of; (1) condensation system; (2) solution containing three-necked flask; (3) thermocouple; (4) magnetic stirrer cum hot plate.

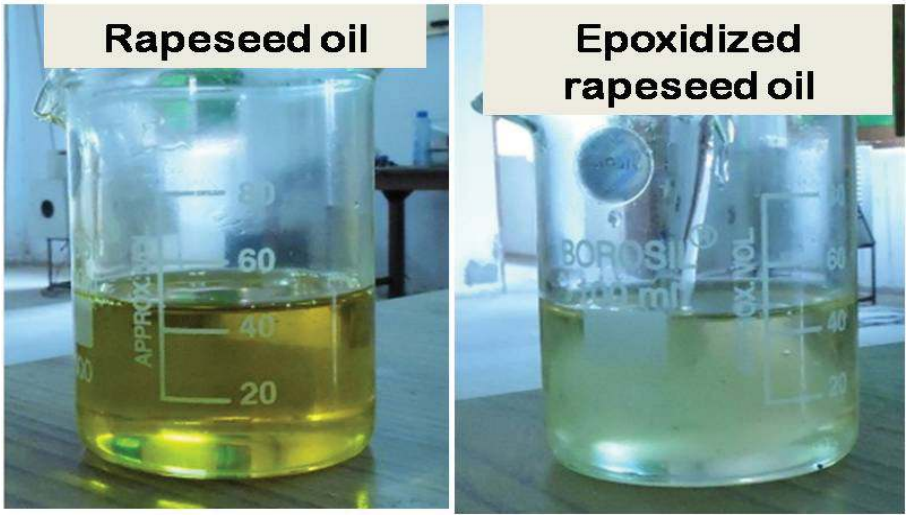

Figure 6.2. Typical image of unmodified and epoxidized oil.

The oil obtained was named as epoxidized rapeseed (ERO), or epoxidized sunflower oil (ESO) or epoxidized castor oil (ECO). Figure 6.2 depicts the typical image of unmodified and epoxidized rapeseed oil. The color of the oil also changed after epoxidation from dark yellow to light yellow. The viscosity and pour point of the epoxidized oils was also improved. The viscosity of the ERO, ESO, and ECO increased from 0.089, 0.076 and 0.28 (unmodified RO, SO and CO) to 0.153, 0.196 and 0.502 N-s/m^2 respectively. However, the viscosity for 0.5%w/v CeO_2 in castor oil and ECO observed as 0.285 and 0.505 N-s/m^2 respectively. It indicates that no significant variation in viscosity was observed with small amount of CeO_2 nano-additives in CO and ECO. Thus, no substantial change was noticed in the estimated film thickness. Also, the slight improvement in pour point observed from -29, -18 and -33 (unmodified RO, SO, CO) to -31, -18 and -37°C for ERO, ESO and ECO respectively.

6.1.2. Characterization of epoxidized oils

The confirmation of epoxidation was done with NMR and FTIR spectroscopy. For NMR, the sample was prepared in deuterated chloroform (99.8%). This is due to non-reactive nature of

deuterated chloroform. It never changes its deuterium with oil molecules proton. FTIR elucidates the characteristic peaks between the wavenumbers 4000-500 cm^{-1}. AOCS Cd 1-25 method (iodine value) was also used to examine the oxidation stability of the modified oils. If the oil has low iodine value it indicates higher amount of saturation thus high oxidation stability and vice-versa.

Each biolubricants possesses both saturation and unsaturation in fatty acid structure. Unsaturation (one or more C=C) restricts the biolubricants for wide use due to poor thermo-oxidative stability. Therefore this shortcoming can reduce or vanished by epoxidation. Proton NMR (^1H) spectra of unmodified and epoxidized oil has shown in Figure 6.3. Different ^1H peaks along with wide range of frequency presented in Table 6.1. It is simply representation of CH_n (n= 0-3) carbons allocation. Unsaturation present in biolubricants was identified with proton spectra at δ 5.1-5.4 ppm (Figure 6.3a, c, e). After epoxidation of oil these characteristic peaks were almost eliminated. And, new proton spectra appeared at δ 3.0-3.2 ppm (Figure 6.3b, d, f). It indicates the formation of oxirane ring (or epoxy group) by altering the C=C structure with -CH- attached with oxygen radical (Adhvaryu and Erhan, 2002). Hence it presumed successful modification of biolubricants by epoxidation process.

FTIR tool was also used for further confirmation of epoxidation (Figure 6.4). It shows unsaturation absorption peaks at wavenumer of 3013, 3008 and 3007 cm^{-1} due to C-H stretch and at 1611, 1643 and 1623 cm^{-1} due to C=C stretch for RO, SO and CO respectively. However after epoxidation these peaks eliminated and new peaks appeared at 828, 835.7 and 839 cm^{-1} in ERO, ESO and ECO respectively. It also interprets the successful epoxidation. Salimon et al. (2011) also reported analogous results for ricinoleic acid representing the formation of quaternary carbons of oxirane ring.

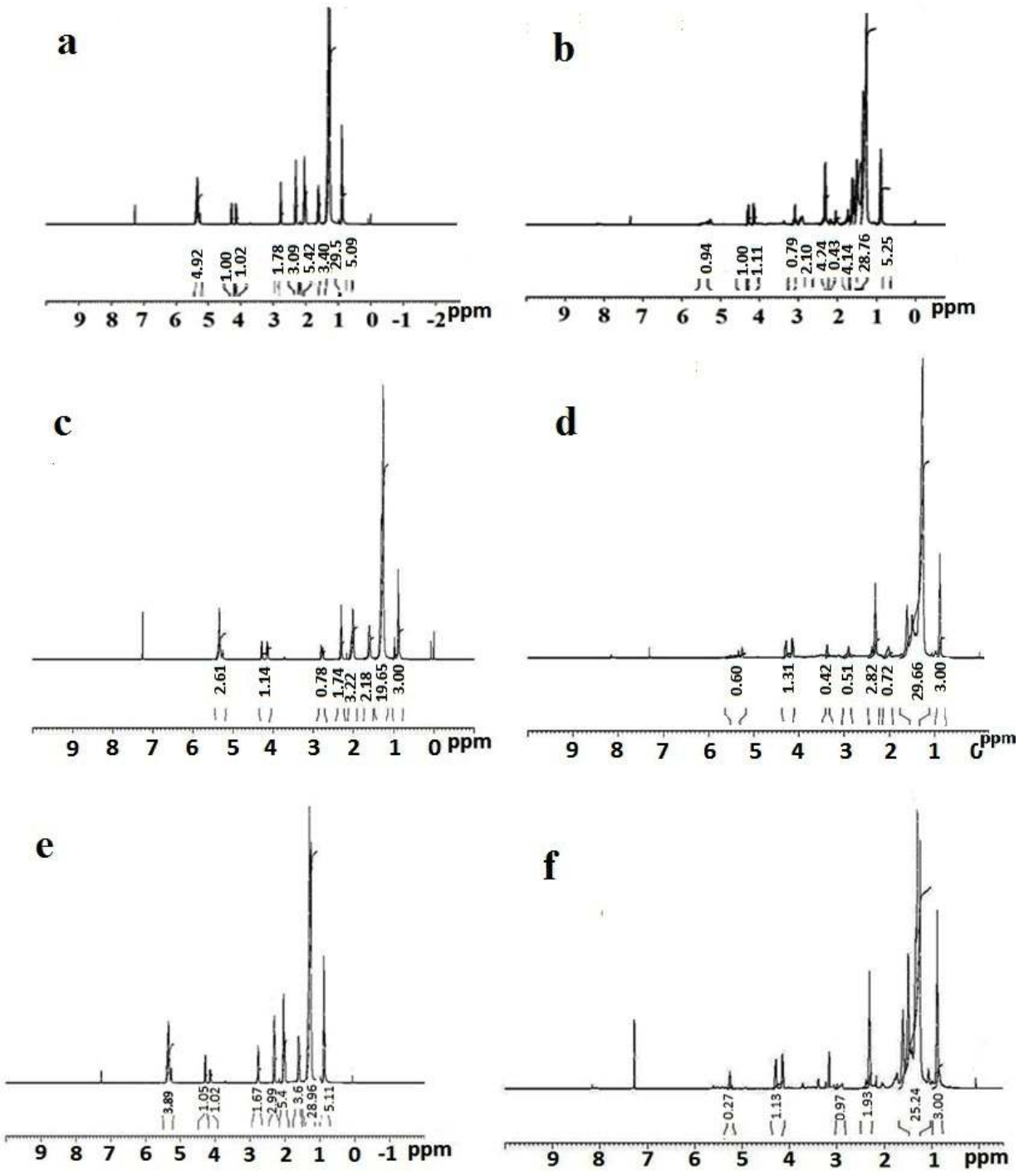

Figure 6.3. Proton NMR of (a) RO, (b) ERO, (c) SO, (d) ESO, (e) CO and (f) ECO.

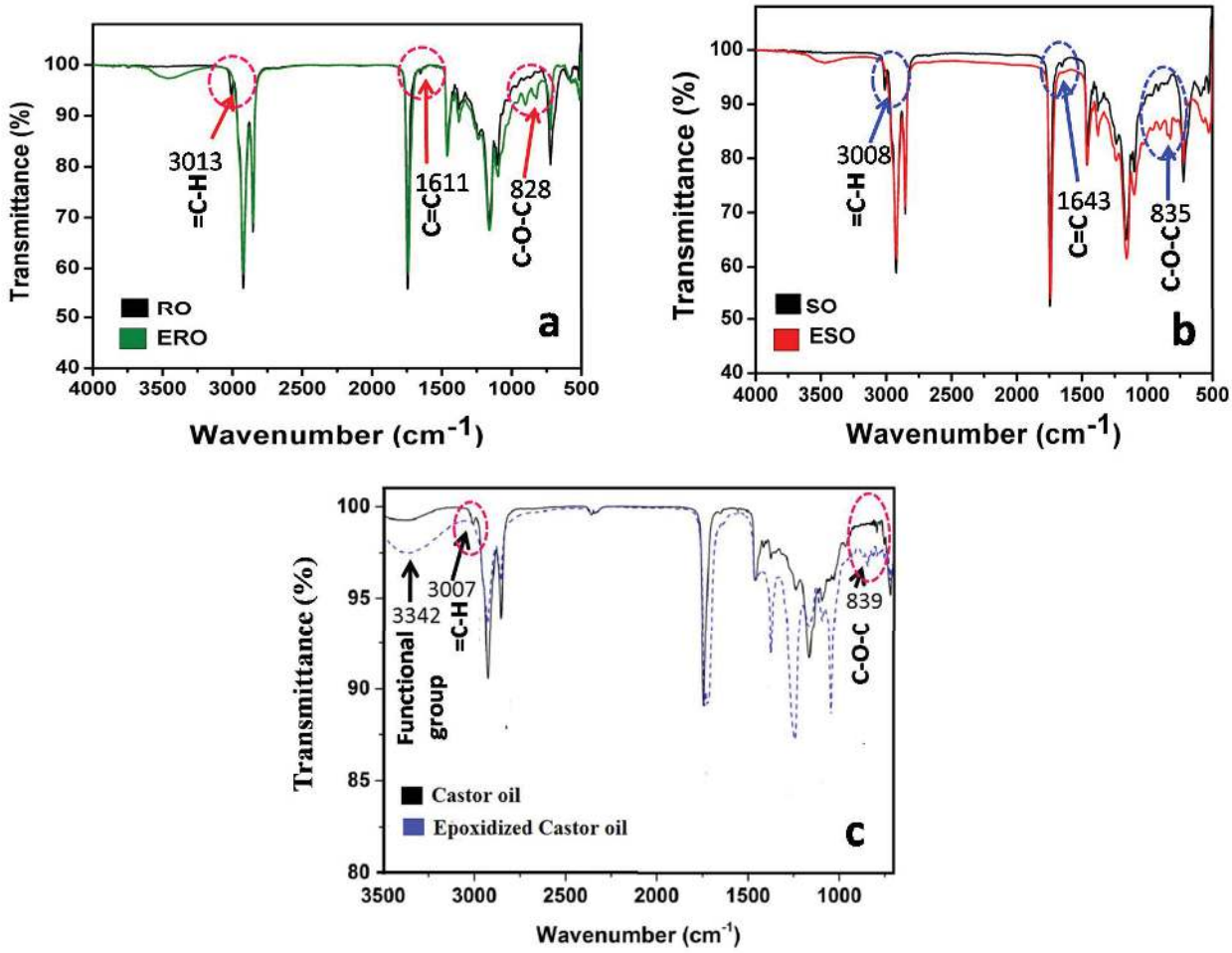

Figure 6.4. FTIR image of (a) RO and ERO, (b) SO and ESO, and (c) CO and ECO.

Table 6.2 enlisted the different absorption phenomena persist for wide frequencies range. A broad peak of O-H (hydroxyl group) was identified at 3350-3420 cm^{-1} frequency range. It is a functional group present in the biolubricant. Further, iodine value test was performed to examine the unsaturation in epoxidized oil. Here, RO, SO and CO shows higher iodine value i.e. 96, 125 and 85 respectively. However, it reduced to 6, 7, and 11 accordingly after epoxidation. Low iodine value represents higher amount of saturates and vice-versa. Thermo-oxidative stability has direct relation with iodine value. One can say, low iodine value of oil has better thermo-oxidation property, thus epoxidized oils better than unmodified oils.

Table 6.1: Summary of proton NMR spectra over the range of frequencies.

Frequency (ppm)	Inferences
δ 5.1-5.4 ppm	Proton of unsaturated carbon (C=C)
δ 4.0–4.4 ppm	Methylene proton of $–CH_2$-CH-CH_2- the backbone
δ 3.0–3.2 ppm	-CH- protons of the epoxy ring
δ 2.8–3.0 ppm	CH_2 proton adjacent to two epoxy group
δ 2.2–2.4 ppm	α-CH_2 a carbonyl group (>C=O)
δ 1.7–1.9 ppm	α-CH_2 the epoxy group
δ 1.55–1.7 ppm	β-CH_2 to >C=O
δ 1.4– 1.55 ppm	β-CH_2 the epoxy group
δ 1.1– 1.4 ppm	Saturated methylene groups
δ 0.8–1.0 ppm	Terminal -CH_3 groups

Table 6.2: Summary of major FTIR absorption frequencies and their inferences.

Characteristic absorption (cm^{-1})	Functional group/ intensity	Inferences
3200-3600	O-H, Broad and strong	Stretching of phenols or alcohols
3000-3100	C-H, medium	Stretch Alkenyl, absorption peaks of unsaturation
2850-3000	C-H, strong	Stretch Alkane
1700-1800	C=O, strong	Stretching of esters
1610-1680	C=C, variable	Stretch, absorption peaks of unsaturation
820-843	C-O stretch, medium	Epoxy oxirane ring stretching

6.2. Comparative evaluation of tribo-performance for unmodified and epoxidized oils

6.2.1. Rapeseed and epoxidized rapeseed oil with different nano-additives

6.2.1.1. Antiwear study of modified and unmodified rapeseed oil

For base oils without additive

The WSD for all RO and ERO compositions summarized in Table 6.3. The SEM images of wear scar tested with RO and ERO shown (at different magnifications) in Figure 6.5. The WSD was reduced to 528.8 µm for ERO from 788.4 µm (RO) without any additive. It ascribed that formation of epoxy group responsible for WSD reduction by 33%. Arumuam and Sriram (2013) reported that the epoxy group have tendency to enhance the adherence and lubricity property by strong physical and chemical adsorption. It reflects the tribo-performance. The variation of 5.6 and 4.3% (for three repeated test) observed in WSD for RO and ERO respectively. A close view of the worn surface reveals fine scratches for RO while shallow groove for ERO. Probably the presence of polar functional group helps in formation of strong tribo-film, which separate metal to metal contact.

Table 6.3. WSD for different RO and ERO compositions.

Wear scar diameter (WSD; in µm)										
Type of oil	***Raw oil***	***Nanoparticle concentration (%w/v)***								
		S-CuO			**CeO_2**			**PTFE**		
		0.1	**0.25**	**0.5**	**0.1**	**0.25**	**0.5**	**0.1**	**0.25**	**0.5**
RO	788.4	710.8	861.4	1052.1	656.6	663.6	736.5	404.0	426.6	682.6
ERO	528.8	804.5	569.1	792.9	485.2	624.8	865.8	700.2	715.0	443.4

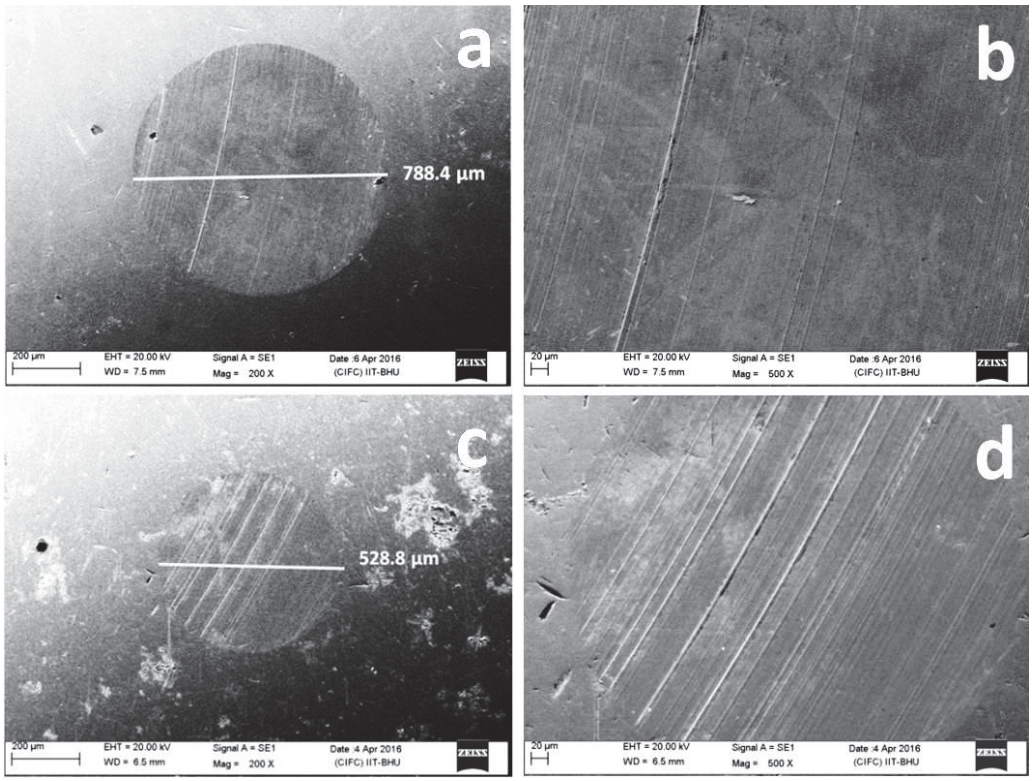

Figure 6.5. SEM morphology of worn surfaces tested at load 392 N for 1h with; (a,b) RO and (c,d) ERO. [b and d at 500x]

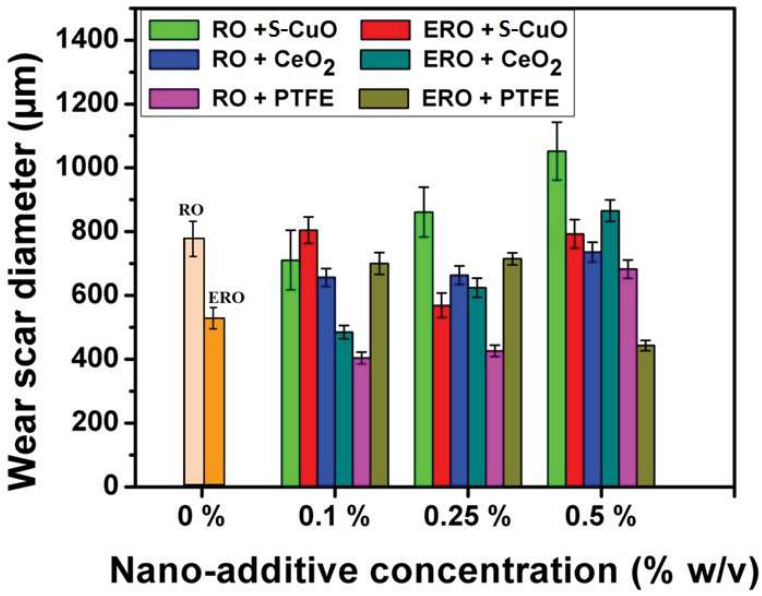

Figure 6.6. Comparative WSD variation with different nano-additive concentrations in RO and ERO tested at 392N load, 1200 rpm speed for 1h.

For nanoparticle based lubricants

The variations in WSD for all RO and ERO compositions have been depicted in Figure 6.6. It was observed that S-CuO base lubricants exhibit more variation in WSD than CeO_2 and PTFE based lubricants. Also, this deviation was higher as compare to the base oil.

Figure 6.7 and 6.8 shows the SEM morphology of wear scar for different RO and ERO compositions respectively. The worn surface topography reveals deep or shallow furrows, scratches, transfer film etc. This is a clear indication that the tribo-system working in the boundary lubrication regime (Ghaednia et al., 2015). For S-CuO base nanolubricants, no wear reduction was observed except at 0.1%w/v concentration (Table 6.3). It indicates that S-CuO nanoparticles were not compatible with RO and ERO. On the contrary, a substantial improvement in WSD observed for CeO_2 and PTFE nanoparticles based nanolubricants. It attributed to morphology along with concentration responsible for such behavior. In literature it is reported that the particles having lower aspect ratio (the ratio of major to minor dimension) may perform better in tribological contacts (Hwang et al., 2011; Dai et al., 2016; Hu et. al. 2010). CeO_2 and PTFE nanoparticles were almost spherical (low aspect ratio) in present study, thus better tribological performance. For CeO_2 in RO and ERO, the WSD was reduced by 16.7 and 8.2% (maximum) with 0.1%w/v concentration respectively. In spite of superior antifriction property of PTFE, an outstanding antiwear performance was also observed as lubricant additive in this study. RO with 0.1%w/v PTFE reduced the WSD by 48.7% compared to the base oil. However, ERO with 0.5%w/v of PTFE reduced it by 16.1%. It elucidates that PTFE has good compatibility with RO and ERO.

Figure 6.9 shows the mean wear volume (MWV) and interfacial shear stress variation for all RO and ERO nanolubricants compositions. The variation of MWV shows almost similar trend as WSD, because MWV calculated with the help of WSD.

The three-dimensional AFM roughness images of worn surfaces tested with different RO and ERO compositions illustrated in Figure 6.10. Figure 6.10a, c and e represents the roughness image of worn surface tested with RO, RO+0.1% w/v CeO_2 and RO+0.1%w/v PTFE respectively and corresponding roughness values were 32, 26 and 25 nm respectively. Also, ERO compositions show higher roughness values. Figure 6.10b and d illustrates the three-dimensional roughness morphology of ERO and ERO+CeO_2 (optimum). The corresponding roughness values were 107 and 806 nm respectively. From the obtained results it is clear that CeO_2 and PTFE have good synergy with RO and ERO than S-CuO nano-additives.

Figure 6.11 shows the typical EDS spectra of worn surfaces tested with S-CuO, CeO_2, and PTFE nano-additives in the base oils. The traces of nanoparticles obtained with significant iron content in few samples. As discussed in the chapter- 5 (section 5.3.1.1), probably, embedment of broken hard and brittle CeO_2 and S-CuO particles or strong adhesion of PTFE nano-additive at the interface may be responsible.

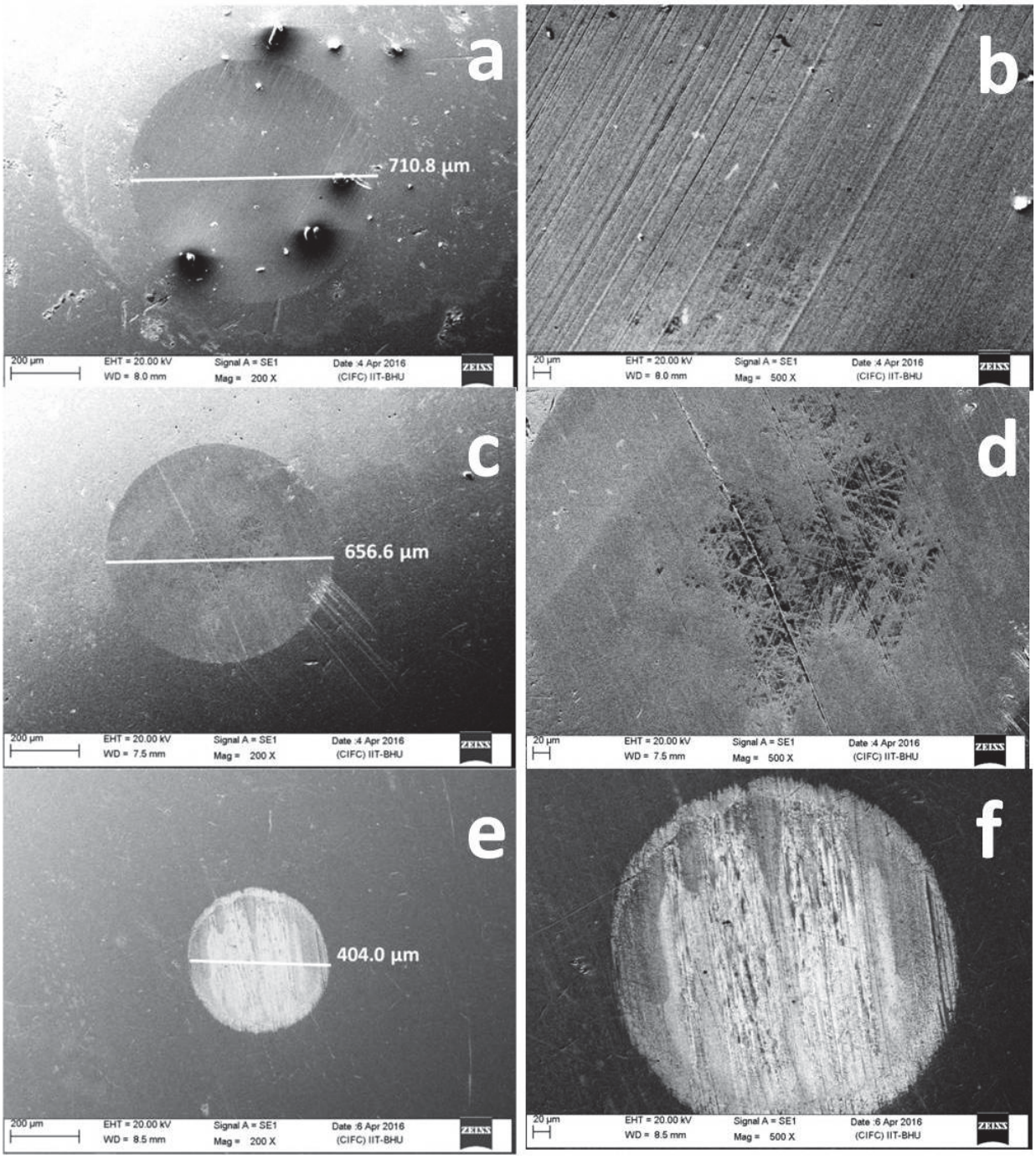

Figure 6.7. SEM morphology of worn surfaces tested with nanolubricants at optimum concentration of; (a, b) S-CuO, (c, d) CeO_2 and (e, f) PTFE nanoparticles in RO with 392N load, 1200 rpm speed for 1h. [b,d and f at 500x]

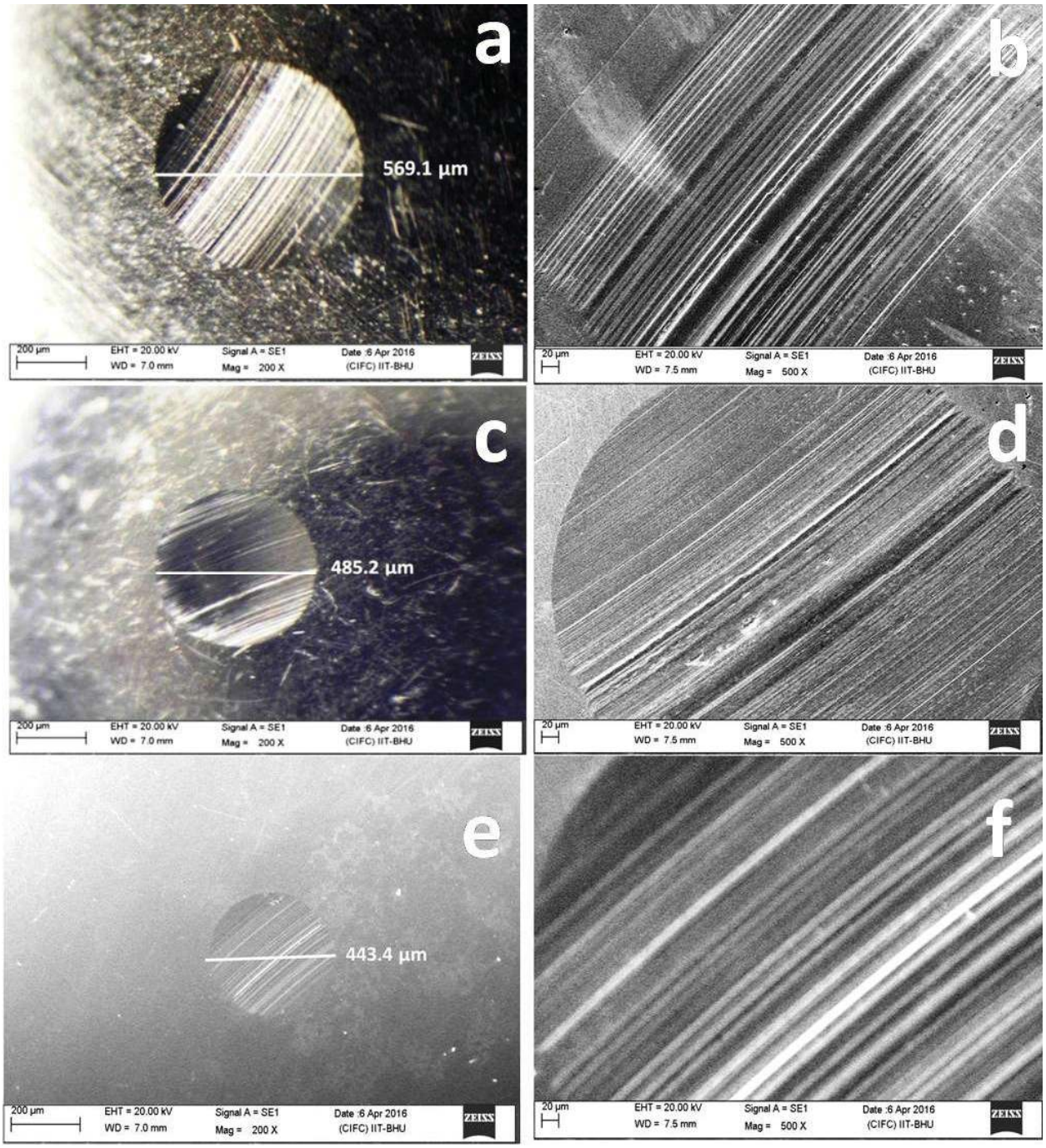

Figure 6.8. SEM morphology of worn surfaces tested with nanolubricants at optimum concentration with (a, b) S-CuO, (c, d) CeO_2 and (e, f) PTFE nanoparticles in ERO with 392N load, 1200 rpm speed for 1hr. [b,d and f at 500x]

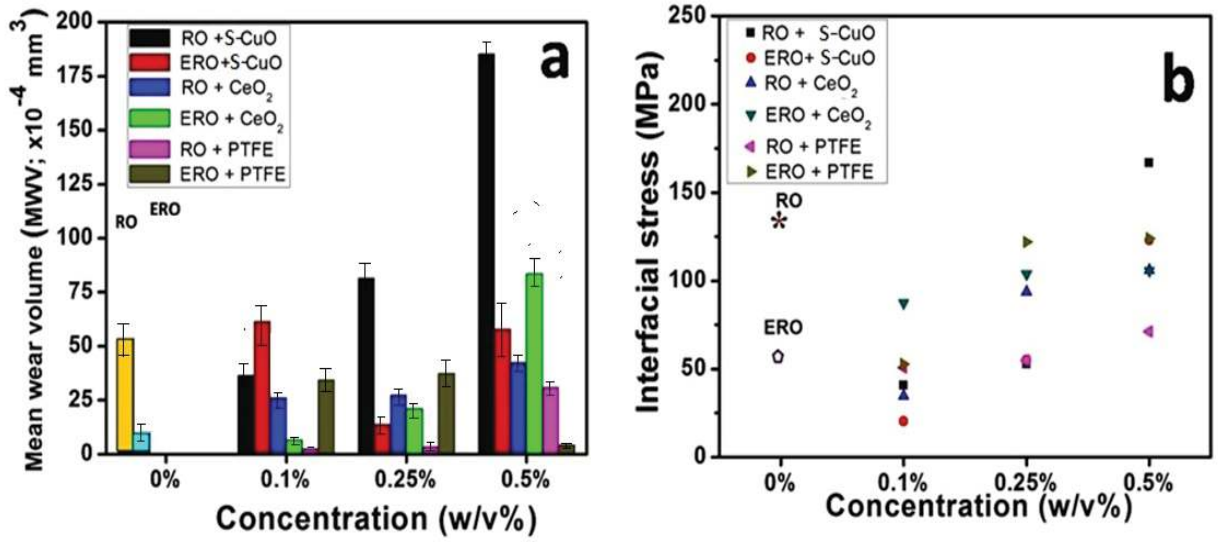

Figure 6.9. Variations in; (a) MWV and (b) interfacial shear stress for different RO and ERO compositions.

Possible mechanism for antiwear

Since 0.1%w/v amount of CeO_2 in RO and ERO provides lowest wear scar, thus considered as optimum concentration. It may due to the presence of threshold number of particles even after squeeze-out action under high contact pressure. Also, a uniform nanoparticle suspension helps in asperity-asperity separation. It is also proposed that under continuous sliding and higher applied load the topmost surface of the nanoparticles get fractured and generates ultrafine secondary particles (Wäsche et al., 2015). These secondary particles along with primary nanoparticles mend the surface dimples and valleys. And, real contact area reduced significantly (Ghaednia and Jackson 2013). Nevertheless, adhesion phenomena were observed at few places caused by transfer layer (Figure 6.7d). Moreover, increment in the WSD was also observed beyond the optimum concentration of CeO_2 in both RO and ERO. This is because third body abrasion takes place on the ball material by hard nano-additive and revealed as ploughing marks (Figure 6.8).

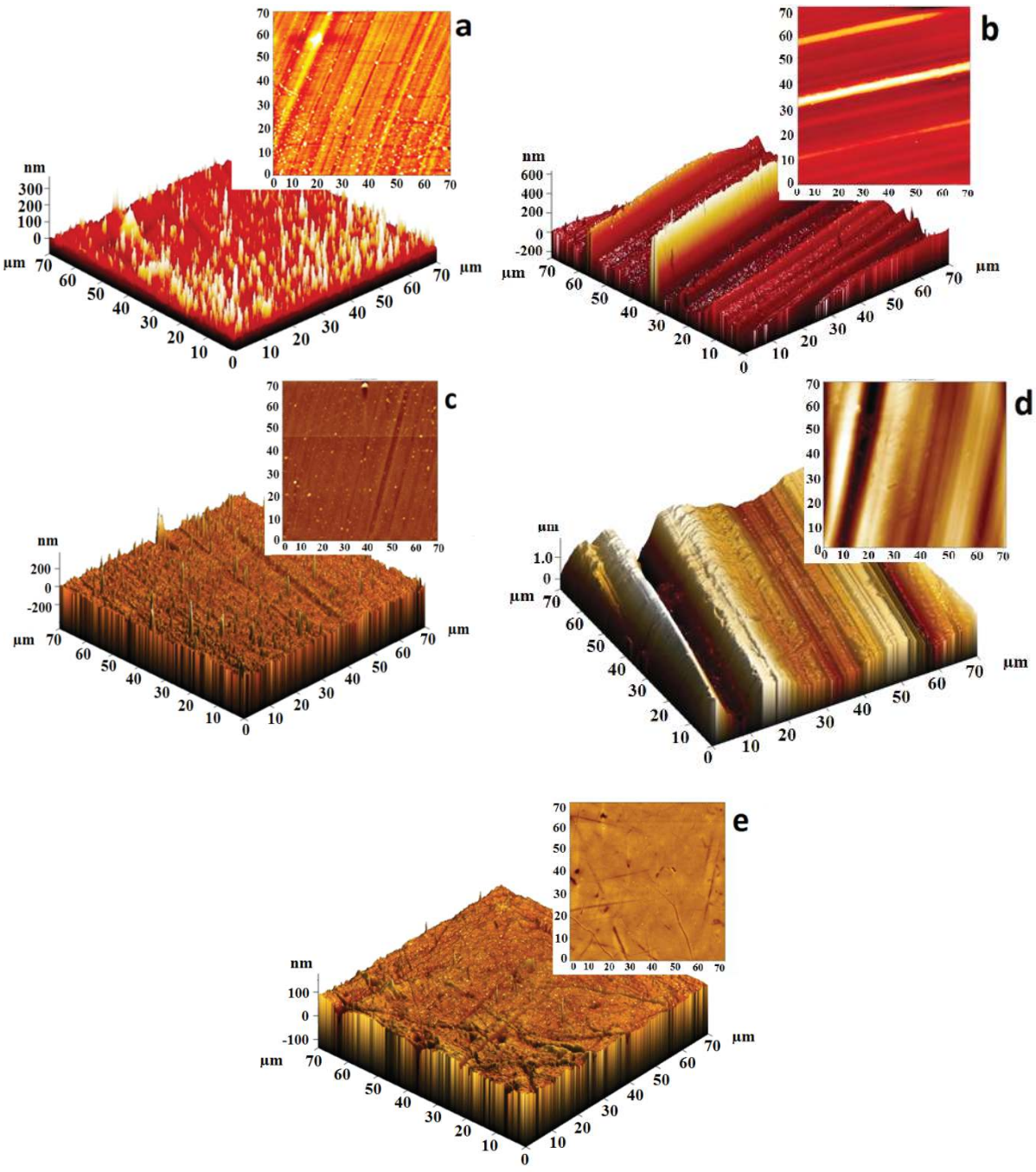

Figure 6.10 SPM roughness images of worn surfaces tested with; (a) RO, (b) ERO, (c) RO with CeO_2, (d) ERO with CeO_2 and (e) RO with PTFE nanoparticles. (load 392N, speed 1200 rpm and time 1h)

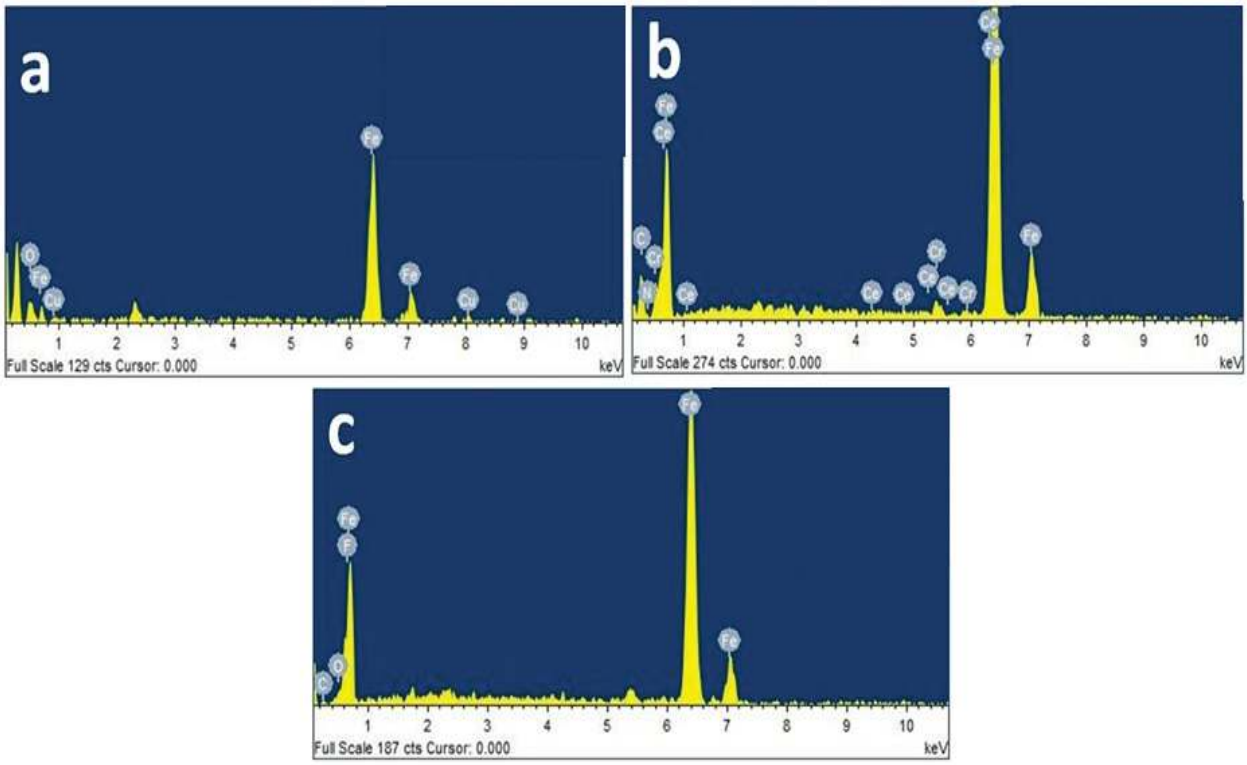

Figure 6.11. EDS spectra of worn surfaces tested with ERO containing (a) S-CuO, (b) CeO_2 and (c) PTFE nanoparticles at optimum concentration.

In case of PTFE in RO and ERO, 0.1 and 0.5%w/v concentration have shown incisive tribological behaviour. Probably, PTFE achieves the activation energy under higher friction heat produced during the sliding (Barry et al. 2015). It results in disintegration of PTFE chain by breaking -C-C- and/or –C-F- bonds (Biswas and Kalyani 1992; Jintang and Hongxin 1988). The disintegrated PTFE react with oxides present on the metallic surfaces or oxygen in the environment, and generates peroxide radicals (Jintang and Hongxin 1988). These oxygen containing radicals have potential to bind PTFE molecules on the contacting surfaces, thus strong adhesion (Biswas and Kalyani 1992). This mechanism is responsible to form denser protective film on rubbing surfaces and have elastic nature. Thus, the contacting surfaces separated to each other and wear performance improved.

6.2.1.2. Antifriction study of modified and unmodified rapeseed oil

The variation in COF for RO and ERO with different nanoparticles is illustrated in Figure 6.12. It is clear from Table 6.4 and Figure 6.12a that RO has higher average friction coefficient than ERO. It may due to the improved lubricity and adhesive property of epoxidized oil in presence of oxirane ring.

Alves et al. (2013) studied the nanoparticles compatibility with different base oils and argued that tribological potential of nanolubricant dependent on oil-additive affinity. The variation in friction coefficient for RO and ERO with each nanoparticles at concentrations 0.1, 0.25 and 0.5 % w/v illustrated in Figure 6.12 b-d. On the basis of obtained friction performance five observations have made. First, the mean COF increases with increase in nano-additive content in both oils (Table 6.4). Second, the lower concentration of S-CuO in RO and ERO was sufficient to provide the improved friction performance. Third, CeO_2 nanoparticles show improved friction property with RO, while impaired with ERO at all the concentration. Fourth, PTFE exhibits better compatibility with RO for all compositions; however ERO improve the friction property at 0.1%w/v only. Fifth, at 0.1w/v% concentration the COF curves are showing near to zero values i.e. ultra-low friction. The presence of oleic and linoleic acid in a fatty acid structure in the biolubricants have a tendency to form a denser monolayer on the mating surfaces and this would have further helped along with the presence of PTFE nanoparticles. At lower concentration of nanoparticles helped to fill the surface valleys and to act as nano-bearing. Therefore, such ultra-low friction behavior was observed.

Table 6.4 summarized the interfacial shear stress and Figure 6.9b shows its variation for each RO and ERO compositions. RO shows interfacial stress as 134.6 MPa, whereas ERO as 58.98 MPa. The nano-additive based RO and ERO reveals similar variation in interfacial

shear stress as that of friction behavior. As discussed in chapter-5 (section 5.3.1.2) that the interfacial shear stress is in direct proportion with COF.

Table 6.4. Summary of mean COF and interfacial shear stress for all RO and ERO compositions with different nano-additives.

Coefficient of friction (COF)										
Type of oil	***Raw oil***	***Nanoparticle concentration (%w/v)***								
		S-CuO			**CeO_2**			**PTFE**		
		0.1	**0.25**	**0.5**	**0.1**	**0.25**	**0.5**	**0.1**	**0.25**	**0.5**
RO	0.066	0.02	0.026	0.082	0.017	0.046	0.052	0.025	0.027	0.035
ERO	0.029	0.01	0.027	0.061	0.043	0.051	0.052	0.026	0.06	0.061
Interfacial Shear stress* (MPa)										
RO	134.6	40.68	52.8	166.7	34.57	93.56	106	50.85	54.9	71.2
ERO	58.98	20.3	55	124.07	87.4	103.7	105.7	52.8	122	124.1
Interfacial shear stress (τ_i) = COF x flow stress of material										

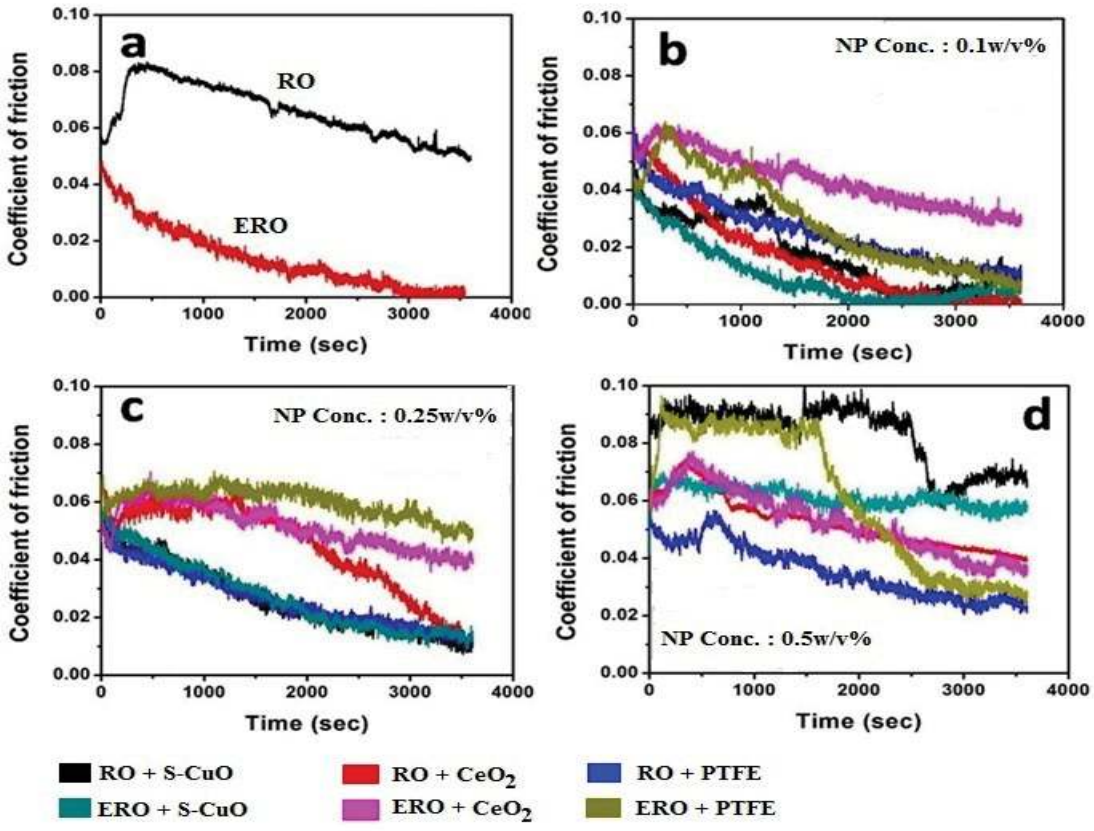

Figure 6.12. Variation in COF for all RO and ERO compositions with S-CuO, CeO_2 and PTFE nano-additives. (load 392N, speed 1200 rpm and time 1h)

Possible mechanism of antifriction

As compared to base oil, S-CuO and CeO_2 nano-additives with RO show minimum COF at lower concentration. This is because optimum number of particles available in contact zone to separate the asperities. Wei and Huaqing (2012) reported that as the amount of nanoparticles increases, attraction among the particles increases which restrict the Brownian motion of the nanoparticles, thus nanoparticle aggregation obtained. These clustered particles act as an abrasive agent. For oxide particles rolling-sliding phenomena and reduction in real area of contact gives improved friction property. In case of PTFE based nanolubricants, when nanoparticles trapped between contacting surfaces then PTFE chain disintegrated. It forms an active group which enhances the reaction rate with the mating surfaces (Harris et. al. 2015). This generates a coherent and strong adhesive transfer film (Biswas and Kalyani 1992). Further interaction of adhered PTFE with metal surface increases the anisotropic deformation. It reflects the proximity of the adjacent chains (Jang et. al. 2007). Therefore, friction was reduced by smooth shearing of these chains (Jang et. al. 2007; Biswas and Kalyani 1992).

6.2.1.3. Extreme-pressure study of modified and unmodified rapeseed oil

Table 6.5 enumerates EP properties of RO and ERO compositions. Both RO and ERO (without additive) show the similar EP performance. Also, no significant improvement in load carrying capacity was observed with low concentration range of oxide particles in RO and ERO. However 0.5%w/v (higher concentration range) improved the load carrying capacity from 126 to 160 kgf. The variation in the nanoparticle size may be responsible for such improvement. As discussed in section 5.3.1.1, Lovell et al. (2010) reported that

bigger sized nanoparticles takes the fractional applied load and separate contacting surfaces, thus improved load carrying properties. Also, smaller particles keep the surface smooth by mending. Under higher sliding speed and load, only higher concentration range was sufficient to separate the rubbing surfaces by providing optimum number of particles even after squeezing out action. Laura et al. (2014) also reported similar EP behaviour with different nanofluids applied in deep drawing, stamping, and metal working process. Further, PTFE did not show any improvement with RO and ERO at either concentration.

Table 6.5. EP performance of all RO and ERO compositions with nano-additives.

Oil composition	***S-CuO***		***CeO_2***		***PTFE***	
Additive concentration (%w/v)	***Last non-seizure load (kgf)***	***Weld load (kgf)***	***Last non-seizure load (kgf)***	***Weld load (kgf)***	***Last non-seizure load (kgf)***	***Weld load (kgf)***
RO (0%)	126	160	126	160	126	160
ERO (0%)	126	160	126	160		
RO+ 0.1%	126	160	126	160		
RO+ 0.25%	126	160	160	200		
RO+ 0.5%	160	200	160	200		
ERO+ 0.1%	126	160	126	160		
ERO+ 0.25%	126	160	126	160		
ERO+ 0.5%	160	200	160	200		

6.2.2. Sunflower and epoxidized sunflower oil with different nano-additives

6.2.2.1. Antiwear study of modified and unmodified sunflower oil

In this section varying concentration of S-CuO and CeO_2 nano-additives were examined with SO and ESO. For the antiwear test, nano-additive concentration optimized based on average

WSD (three repeated test). The variation of WSD and MWV for each additive composition has illustrated in Figure 6.13 and Table 6.6.

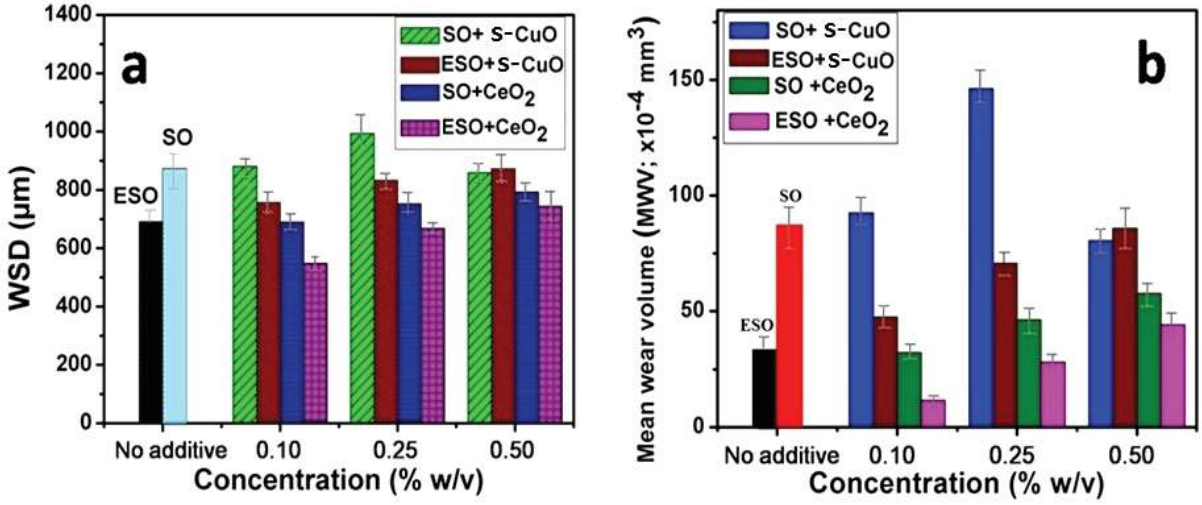

Figure 6.13. Variation of (a) WSD and (b) MWV with different SO and ESO compositions.

The modification of SO dramatically decreased the WSD. It attributed that after epoxidation the interaction between metal surface and oil molecules increased due to alteration from C=C to epoxy ring. ESO reduced the WSD by 20.9% (i.e. from 873 to 690.6 µm) compared to SO. Also, the use of nano-additives influenced the antiwear property significantly. S-CuO nanoparticles shown impaired antiwear property with both SO and ESO at either concentrations (Figure 6.13a). Although, slight reduction in WSD was observe for SO+0.5% S-CuO, but not sufficient to presumed as optimum. On the contrary, outstanding antiwear performance observed with CeO_2 nano-additives in small amount. For both SO and ESO, gradual increment in WSD was noticed with increment in the concentration. With both the oils CeO_2 nanoparticles show lowest WSD at 0.1%w/v, thus assumed as optimum. It speculated that due to smaller size range of CeO_2 exhibits longer and uniform suspension. Thus, lower concentration i.e. 0.1% sufficient to provide threshold particles at contact zone

to keep the mating surfaces away (Ghaednia and Jackson, 2013). Moreover, higher amount of particles shows detrimental the antiwear property.

Table 6.6. Summary of WSD and MWV for different SO and ESO compositions.

WSD (µm)							
Base oil	***No additive***	***Nanoparticle concentration (%w/v)***					
		S-CuO			**CeO_2**		
		0.10	**0.25**	**0.50**	**0.10**	**0.25**	**0.50**
SO	873.0	888.1	993.2	858.9	689.8	752.5	792.7
ESO	690.6	756.7	832.4	872.1	548.1	668.3	743.8
MWV ($x10^{-4}$ mm^3)							
SO	86.2	92.5	146.3	80.5	32.1	46.4	57.7
ESO	32.3	47.5	70.7	85.8	11.6	28.1	44.2

Figure 6.14 shows SEM micrographs of damaged surfaces tested with SO and ESO at optimum S-CuO and CeO_2 concentrations. Base oils (without additive) depicts the deep furrows, trenches, and scratches on the mating surfaces (Figure 6.14a and b). ESO shows better interaction with metal surface in presence of epoxy group. Nevertheless, Figure 6.14b reveals some transfer film. It may due to contact fatigue and adhesive fatigue (Peng et al., 2009). The small nano-additive content in base oil is able to separate the asperities up to a certain extent. In this aspect comparative smoother worn track obtained for nanolubricants and presented in Figure 6.14c-f. At optimum concentration of S-CuO in SO and ESO, shallow furrows and micro-grooves observed (Figure 6.14c and d). In addition, CeO_2 in SO and ESO at optimum concentration (0.1%w/v) also shows smoother and intermittent scratches (Figure 6.14e and f).

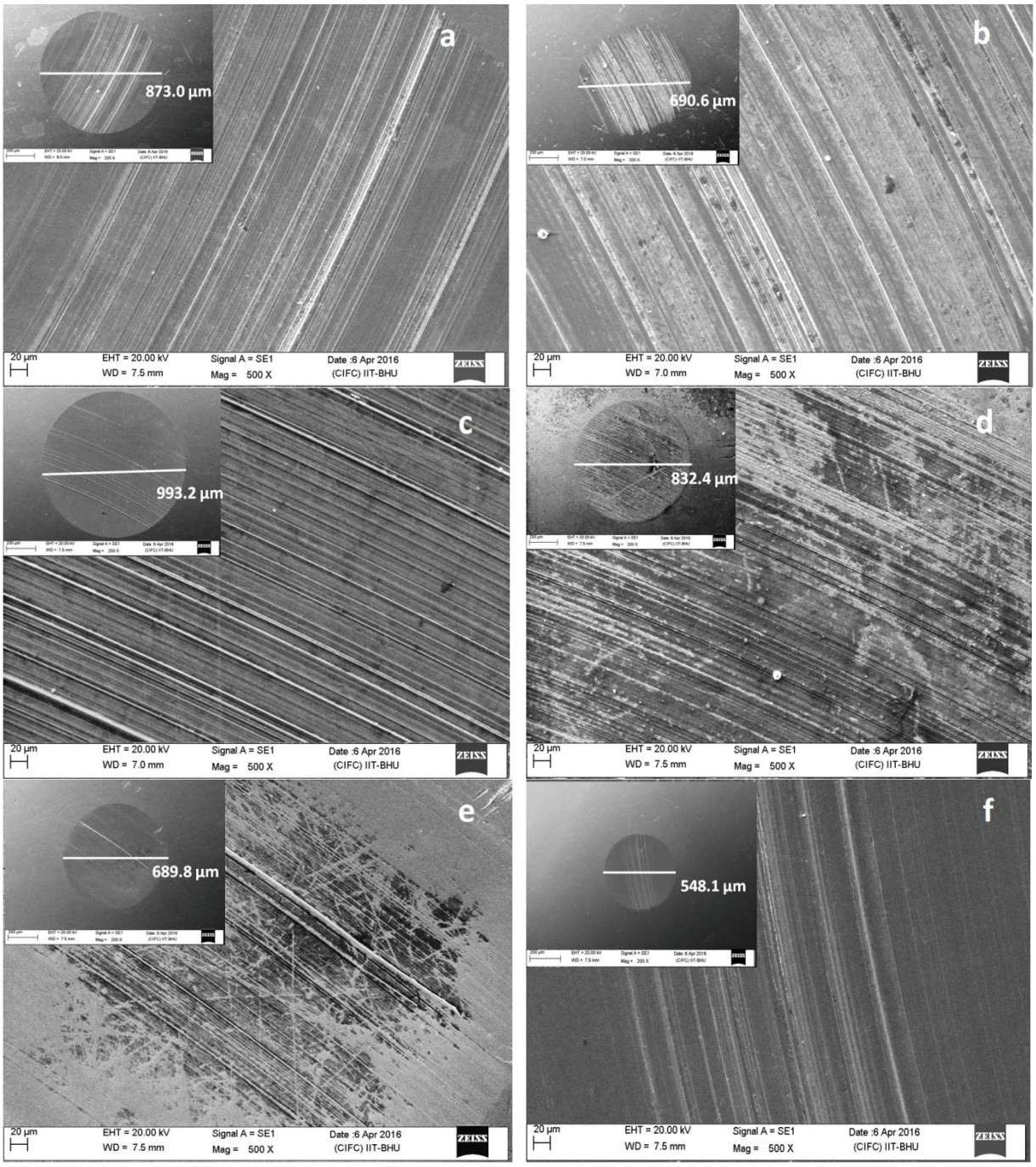

Figure 6.14. SEM micrographs of worn surfaces tested with (a) SO (b) ESO (c) SO + 0.25%w/v S-CuO (d) ESO + 0.10%w/v S-CuO (e) SO + 0.10%w/v CeO_2 and (f) ESO +0.10%w/v CeO_2. (load 392N, speed 1200 rpm and time 1h)

Due to contact fatigue nanoparticles itself start to fracture under sliding and generates the tiny particles as debris (Wäsche et al. 2015). These tiny particles act as filler and help the nano-additives in surface smoothening. It also avoids asperity-asperity contact, thus improvement in antiwear properties. The good compatibility of CeO_2 nanoparticles in SO and ESO was also confirmed by the worn surface topography (SEM) as compare to S-CuO.

EDS spectra of the rubbed surfaces are presented in Figure 6.15. The minute traces of Cu and Ce revealed on the worn track in few samples. It may result of entrapment of S-CuO and CeO_2 during sliding. The oxygen in the EDS spectra may result of oxide particle or epoxy product.

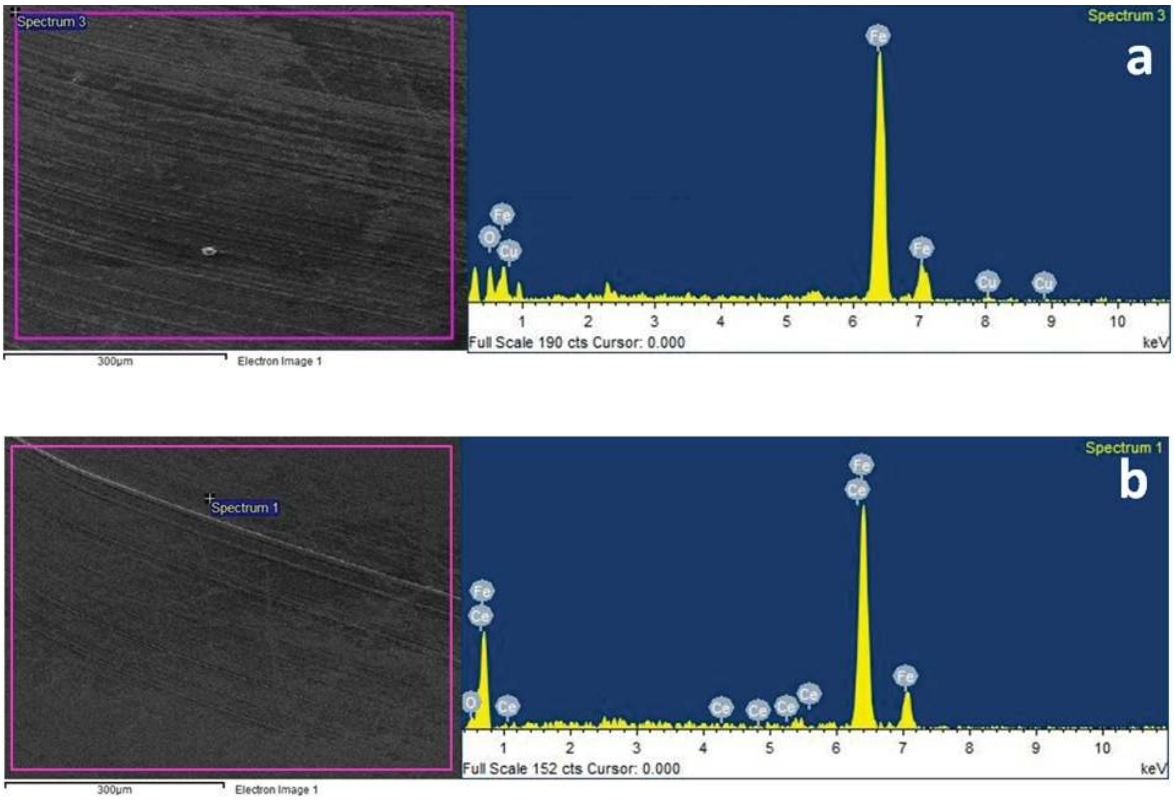

Figure 6.15. Typical EDS spectra of worn surfaces obtained with (a) S-CuO and (b) CeO_2 based nanolubricants.

Figure 6.16 shows roughness morphology of the worn surfaces at optimum concentration. The higher roughness value (R_q) was observed for base SO (260.8 nm) and ESO (466 nm). However, the lowest concentration (0.1%w/v) decreased R_q substantially with both base oils. The roughness value shows in line variation with the SEM results for CeO_2 based nanolubricants. The lower concentration of CeO_2 nanoparticles in SO and ESO elucidates better compatibility than higher concentrations, and it is also confirmed by SPM results. 0.1% CeO_2 in SO and ESO gives R_q value of 70.9 and 60.1 nm respectively. This indicates that roughness was reduced by fourfold and seven-fold than the SO and ESO respectively.

Mechanism of antiwear

It is known that each surface possesses numerous asperities, dimples, and valleys. In the case of close sliding contacts, the tribo-film formed by the lubricant becomes thinner. It promotes the asperity-asperity collision. Therefore nanoparticles assist the base lubricants in such situations. One can say that nanoparticles take fractional loads and reduce/avoid adhesion (Li et al., 2006).

The following three mechanisms may involve in achieving the enhanced antiwear performance; (i), melting and adherence of nano-additives on the rubbing surface to form protective film; (ii), nano-bearing effect of the nanoparticles and (iii) tribosinterisation of the nano-additives on the contact zone (Jaiswal et al., 2014). Since the melting temperature of the oxide particles are very high (more than 1000°C), thus first one can be neglected. Second and third mechanisms i.e. nano-bearing phenomena and tribosinterisation action may participate (either alone or simultaneously) in the contact zone to reflect the tribo-performance as discussed in detail in section 5.3.1.1 and 5.3.3.1 (Chapter-5) respectively.

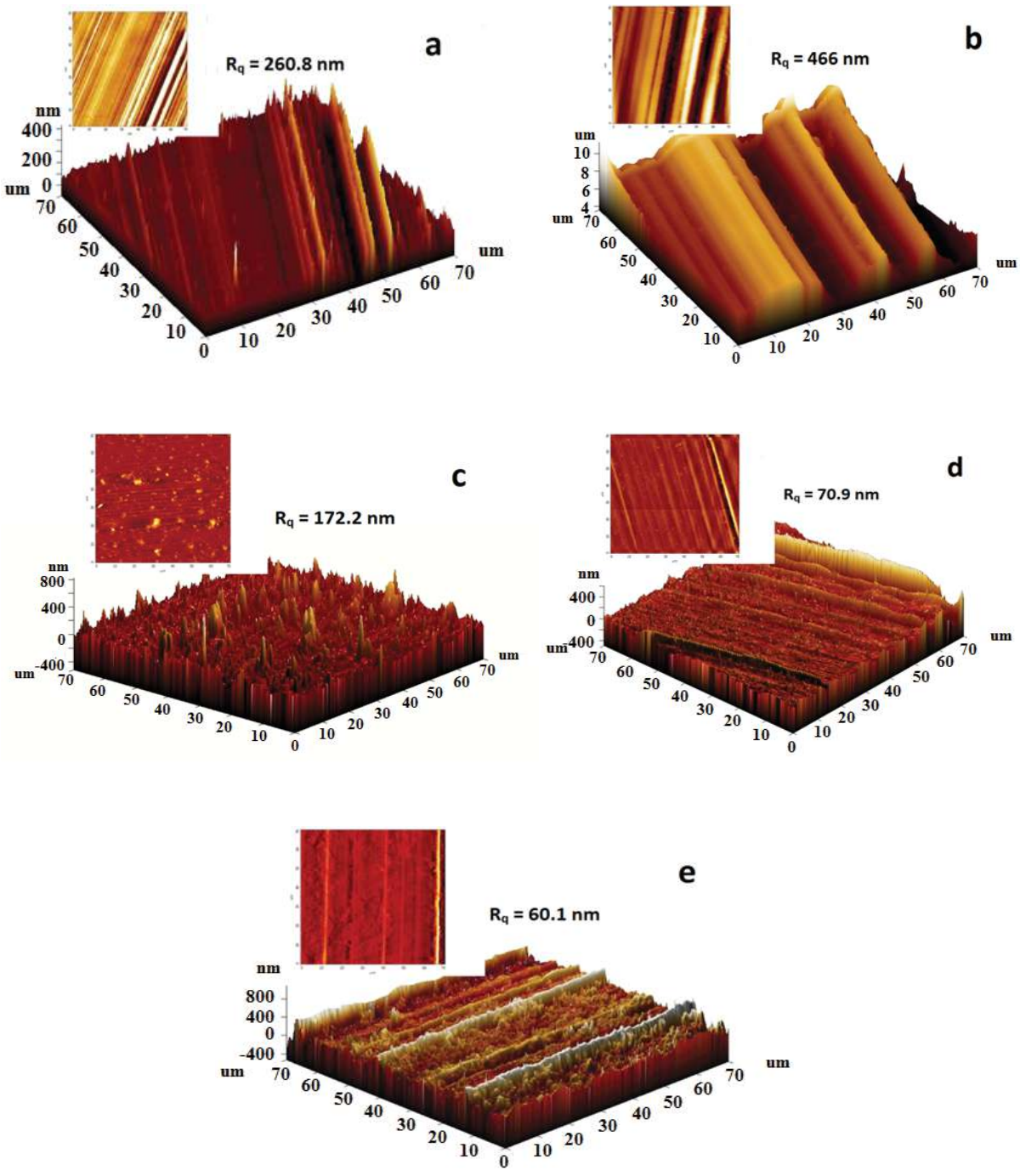

Figure 6.16. SPM roughness images of the worn surfaces tested with (a) SO (b) ESO (c) SO + 0.10%w/v S-CuO (d) SO + 0.10%w/v CeO_2 and (e) ESO + 0.10%w/v CeO_2. [load 392N, speed 1200 rpm and time 1h; Inset: 2-D image of corresponding image]

6.2.2.2. Antifriction study of modified and unmodified sunflower oil

Figure 6.17 and Table 6.7 represents friction variation and their average magnitude for different nanoparticle concentrations, respectively. As compared to SO, the mean COF was reduced by fifty percent for ESO (Figure 6.17a and Table 6.7). Perhaps epoxy group present in ESO promotes the oil-metal interaction and form denser adsorbed layer at the interface. However, nano-additives changed the lubricant performance dramatically. Overall two distinct variations in the COF were observed by varying the concentration. First, lowest concentration (i.e. 0.1%w/v) exhibits continuous decrement in COF up to the asymptotic value for all SO and ESO compositions (Figure 6.17a). Second, 0.25 and 0.5%w/v concentration of oxide nanoparticles reveals either constant or increasing trend of COF (Figure 6.17b-c). It was also noticed that each concentration of CeO_2 with ESO decreased the friction coefficient up to the asymptotic value.

Table 6.7. Summary of mean COF and interfacial shear stress for different SO and ESO compositions.

COF (Avg.)							
Base oil	***No additive***	***Nanoparticle concentration (%w/v)***					
		S-CuO			**CeO_2**		
		0.10	**0.25**	**0.50**	**0.10**	**0.25**	**0.50**
SO	0.0628	0.0296	0.0506	0.0759	0.0488	0.0574	0.0713
ESO	0.030	0.0655	0.0593	0.0646	0.0265	0.0278	0.0273
Interfacial stress (MPa)							
SO	127.7	60.2	102.9	154.3	99.3	116.7	145
ESO	59.1	133.2	120.6	131.4	53.9	56.5	55.5

S-CuO nano-additive provides the lowest COF with 0.1% amount in SO, thus optimum. However impaired friction obtained at all S-CuO composition with ESO. In addition, lower CeO_2 content in SO and ESO improved the COF significantly, which moderately increase with concentration. Therefore, 0.1%w/v CeO_2 presumed as optimum with both SO and ESO.

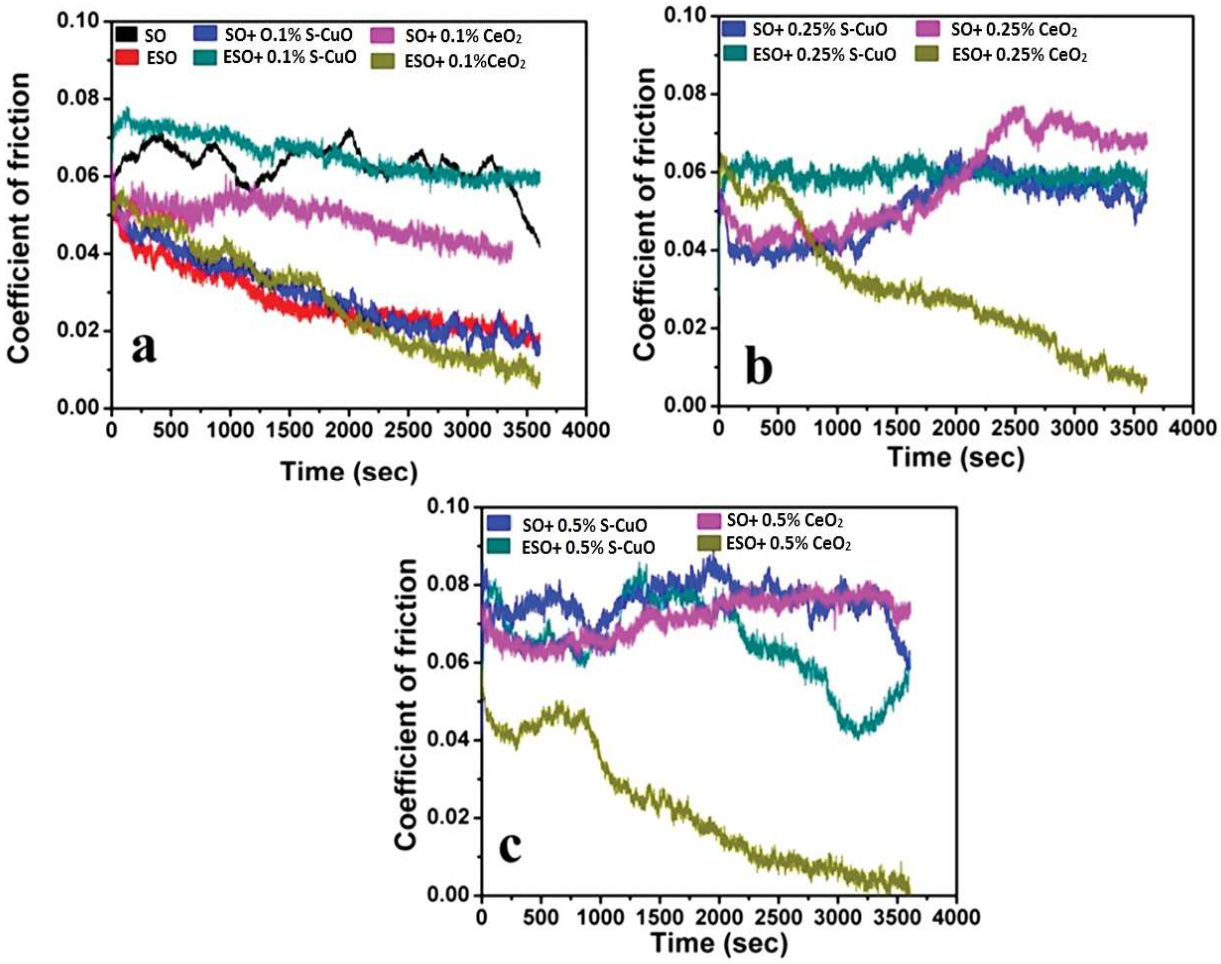

Figure 6.17. Variation in COF for SO and ESO lubricants containing different nano-additives in amount of (a) 0.10 %w/v, (b) 0.25%w/v and (c) 0.50 %w/v. (load 392N, speed 1200 rpm and time 1h)

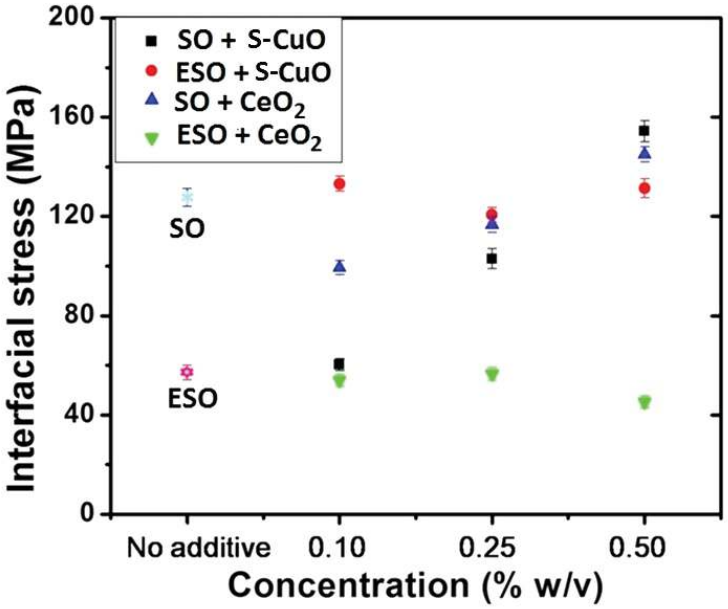

Figure 6.18. Variations in interfacial shear stress for all SO and ESO compositions.

Figure 6.18 illustrates the variation in interfacial shear stress and Table 6.7 provides corresponding values. ESO reveals reduced interfacial stress of 59.1 MPa as compared to SO (127.7 MPa). Also, S-CuO and CeO_2 based nanolubricants shows good agreement between friction coefficient and interfacial stress variation, because of direct proportionality.

Antifriction mechanism

Figure 6.19 represents a typical tribological model having ball-on-ball configuration just like four ball tester. In case of elastohydrodynamic lubrication, adsorbed and ordered layer have imperative role in improving the tribo-performances. However, in dynamic close contact conditions the role of adsorbed layer dominates over the ordered layer. Due to the strong adhesion between the oil molecules and surface, this adsorbed layer behaves like solid. And, loosely bonded oil molecules form mono- or multi-level ordered layer over the adsorbed layer. The ratio of ordered layer to total film thickness will be higher for thin tribo-film. Thus

higher amount of ordered layer in the tribo-film plays a vital role to reflect tribological properties. Also, if these ordered layers ruptured under sliding conditions then only adsorbed layer has a crucial role to protect the surface. The later phenomenon frequently experienced with the boundary lubrication regime (Peng et al., 2009).

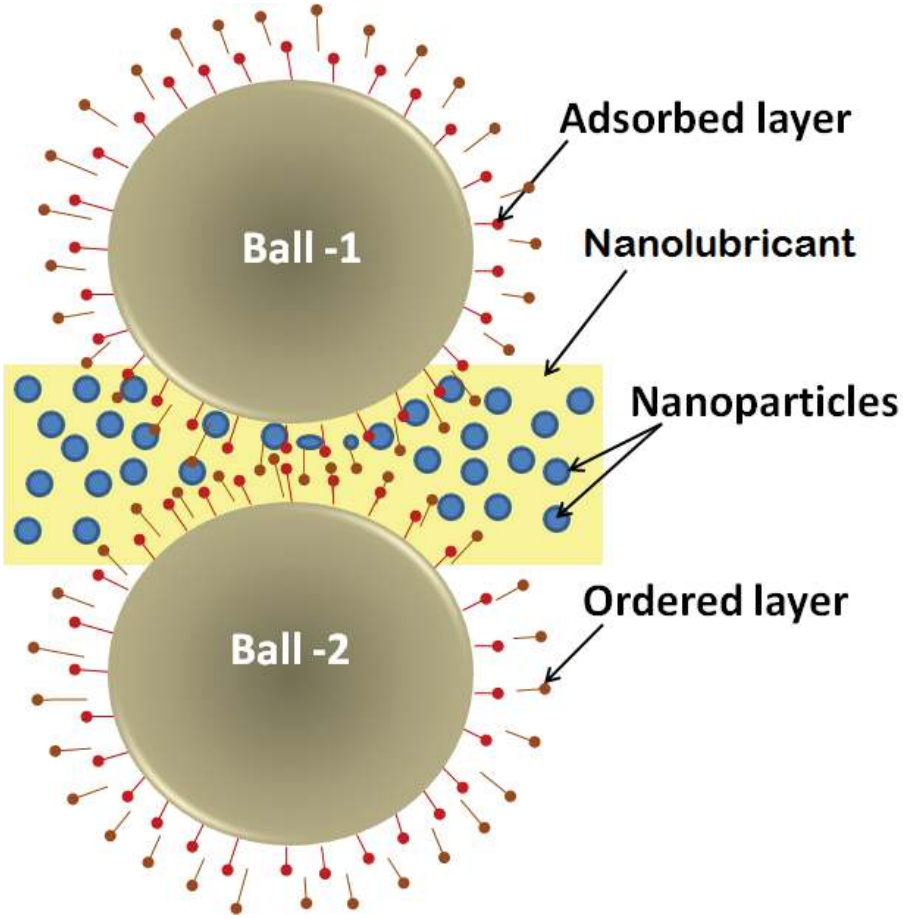

Figure 6.19. Proposed in-situ mechanism for tribological contacts containing nanolubricant to improve tribo-performance in boundary lubrication regime.

If the nanoparticles used in the base oil then one additional layer formed at the interface i.e. nanoparticle's layer. In general, physisorption and chemisorption reactions between metal and oil are responsible in continuous formation of adsorbed layer. In case of epoxidized oil newly formed epoxy group catalyzes the interaction between oil molecule and metallic surface. The nano-additives in lubricant repair the damaged surface by mending action. The nanoparticle's layer carry partial load and separates the mating surfaces simultaneously. But, these conditions are viable up to the optimum amount of nano-additive. If the nano-additive amount goes beyond the optimum level, the deterioration of the surface starts by abrasion mechanism. It causes worse tribo-performance. The damage of surface and sub-surfaces by the nanoparticles under higher load and speed are discussed in detail in the section 5.3.3.2 (Chapter-5).

6.2.2.2.1. Compatibility of nano-additives with SO and ESO

The compatibility of S-CuO and CeO_2 nano-additives in SO and ESO presented in Table 6.8, based on tribological results. The addition of nanoparticles in oil provides both improved and impaired tribological performance. In the present study, good compatibility was observed for CeO_2 nanoparticles with both SO and ESO. However, S-CuO nano-additive shows almost incompatible behavior. Possibly, nanoparticle size may be the one of the responsible factor. Here, CeO_2 nanoparticles were almost 1.5 times smaller than the S-CuO nanoparticles. Therefore, under the influence of the gravity S-CuO nanoparticles rapidly tend to aggregate. In turn, cluster may form in contact zone which impair the tribological properties. On the contrary, smaller CeO_2 nanoparticles dispersed in biolubricant for longer time thus reflect the improved tribo-pair interaction.

Table 6.8. A comparative summary of nano-additive compatibility with SO and ESO.

Nanolubricant	Compatible		Compatibility intensity	Wear	Friction
	Yes	*No*			
SO+ 0.10%CeO_2	✓	✖	High	↓	↓
SO+ 0.25%CeO_2			Moderate	↓	↓
SO+ 0.50%CeO_2			Low	↓	↑
ESO+ 0.10%CeO_2	✓	✖	High	↓	↓
ESO+ 0.25%CeO_2			Moderate	↓	↓
ESO+ 0.50%CeO_2			Low	↑	↓
SO+ 0.10%S-CuO	✖	✓	None	↑	↓
SO+ 0.25%S-CuO			None	↑	↓
SO+ 0.50%S-CuO			Very low	↓	↑
ESO+ 0.10%S-CuO	✖	✓	None	↑	↑
ESO+ 0.25%S-CuO				↑	↑
ESO+ 0.50%S-CuO				↑	↑
↑ : Increase; and ↓: Decrease					

6.2.3. Castor and epoxidized castor oil with different nano-additives

6.2.3.1. Antiwear study of modified and unmodified castor oil

A comparative summary of tribological properties enumerated in Table 6.9. It observed that only by epoxidation of CO, the WSD reduced from 906.4 to 706.6 µm. In other words, 22.04% reduction in WSD obtained for ECO. SEM topography of worn surfaces tested with CO and ECO at different magnifications (100x and 2000x) presented in Figure 6.20. As compared to the CO, ECO shows somewhat smoother morphology. It indicates that

formation of oxirane ring in ECO helps in the formation of the rapid and thicker protective film.

The addition of the nanoparticle in both base oils i.e. CO and ECO substantially reflect the tribological properties. In Table 6.9 wear reduction (WR) was calculated by considering 906.4 and 706.6 µm as reference size separately for CO and ECO compositions. In case of CO with S-CuO, the maximum WSD reduction was 24.04%; thus optimum concentration was 0.1%w/v. A small increment in S-CuO concentration beyond optimum level, impaired antiwear properties observed.

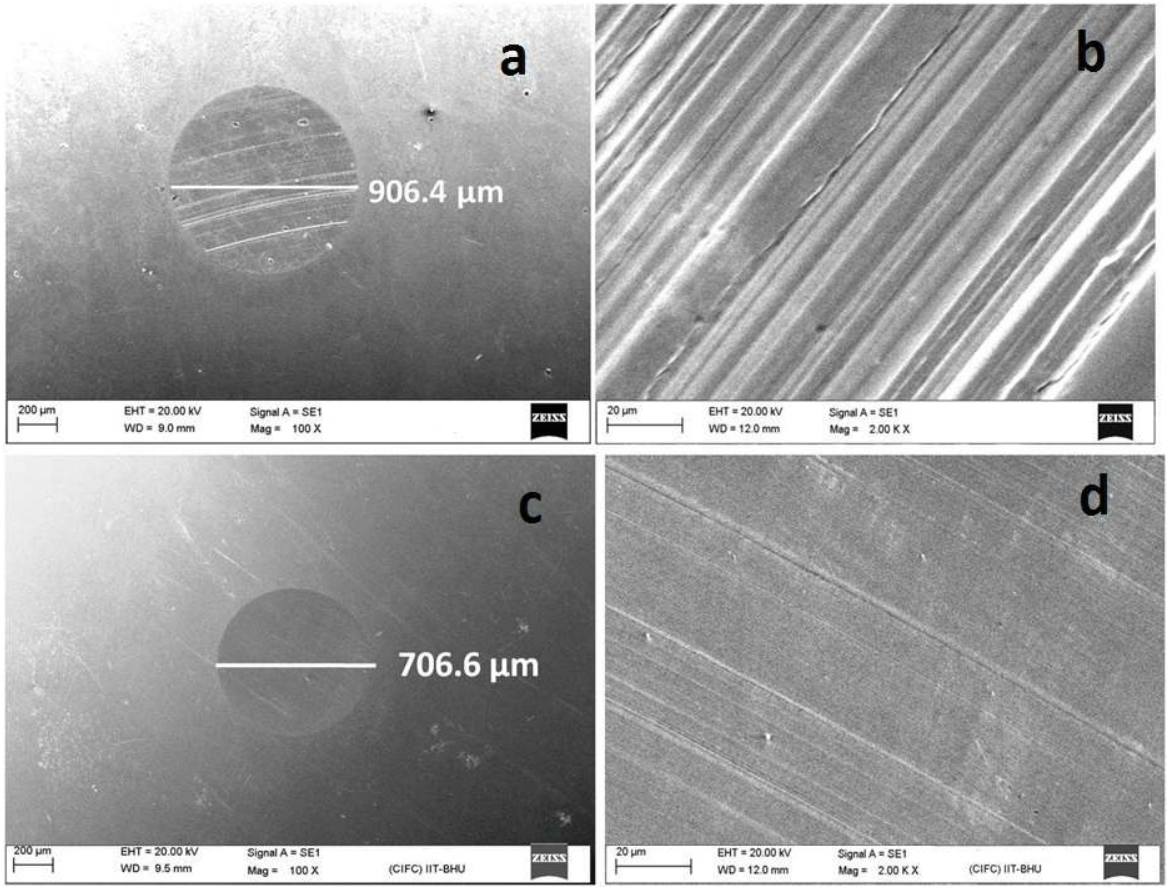

Figure 6.20. SEM images of worn surfaces lubricated with (a, b) CO and (c, d) ECO at different magnification. (load 392N, speed 1200 rpm and time 1h)

Table 6.9. Summary of tribo-properties for all CO and ECO compositions.

Oil compositions	WSD (µm)	WR (%)	MWV (x10^{-4} mm^3)	Specific wear rate (x10^{-17} m^3/N-m)
CO	906.4	-	100.5	3.79
CO+0.1%S-CuO	688.5	24.04	31.9	1.20
CO+0.25%S-CuO	773.4	14.67	52.1	1.96
CO+0.5%S-CuO	817.4	9.82	65.6	2.47
CO+0.1%CeO_2	861.3	4.97	81.5	3.07
CO+0.25% CeO_2	598.8	33.93	17.4	0.655
CO+0.5% CeO_2	732.4	19.2	41.4	1.56
CO+0.1%PTFE	621.2	31.46	20.4	0.77
CO+0.25%PTFE	632.8	30.2	22.2	0.84
CO+0.5%PTFE	635.7	29.86	22.6	0.85
ECO	706.6	-	35.6	1.34
ECO+0.1%S-CuO	587.5	16.85	15.9	0.6
ECO+0.25%S-CuO	739.0	-4.58	43.0	1.62
ECO+0.5%S-CuO	813.7	-15.1	64.4	2.43
ECO+0.1% CeO_2	568.3	19.57	13.8	0.52
ECO+0.25% CeO_2	611.2	13.5	19.0	0.72
ECO+0.5% CeO_2	667.4	5.54	27.9	1.05
ECO+0.1%PTFE	688.1	2.6	31.8	1.2
ECO+0.25%PTFE	686.5	2.9	31.5	1.18
ECO+0.5%PTFE	508.2	28.1	8.2	0.31

CeO_2 and PTFE with CO reduced the WSD by 33.93 and 31.46% at 0.25 and 0.1%w/v concentration respectively. Due to lowest WSD these concentrations was considered as

optimum for CO compositions. At the highest concentration, all CO composition revealed worse property. However, for ECO compositions distinct behavior was observed. S-CuO, CeO_2 and PTFE in ECO reduced the WSD (maximum) by 16.85, 19.57 and 28.1% at the concentration of 0.1, 0.1 and 0.5%w/v respectively. Thus these are the optimum concentration in ECO. One can also say that these are additional reduction in CO after epoxidation and thereafter use of nanoparticles. Figure 6.21 and 6.22 represents the SEM and SPM roughness images of the worn track obtained at optimum concentrations of the nanoparticles in ECO only (because all nano-additives in CO explained in chapter-5).

It is clear from the obtained result that ECO with lower concentration range i.e. 0.1%w/v improved the antiwear behavior substantially while polymeric particle (PTFE) shows improvement at higher concentration range. Arumuam and Sriram (2013) reported that the formation of the epoxy group has the propensity to enhance the adherence and lubricity property by strong physical and chemical adsorption. Also, the increased viscosity after epoxidation catalyzes nanoparticle suspension stability and this has facilitated for mending, rolling, and polishing effect during the sliding (discussed in chapter-5). As the viscosity of the oil increased after epoxidation, it may help the nanoparticle to disperse uniformly for longer time as compared to unmodified oil. Also, change in the chemical structure of fatty acid chain increase the affinity of the oil molecule towards the metal surface. Up to the optimum concentration the mating surfaces separated by the nanoparticles protective film and thick adsorbed and ordered layer of oil molecules. Figure 6.21 reveals the smoother surface as compared to the base oils, which justifies the made hypothesis. Higher concentration of nanoparticle impairs the tribo-performance even inferior than the base oils. The obtained roughness value shows 46.4% reduction in R_q (from 398.5 to 213.4 nm) for

ECO as compared to CO. However as compared to the ECO, the formulated oil i.e. ECO with S-CuO, CeO_2 and PTFE at optimum concentrations reduced the line roughness 9.3, 54.5 and 57.9%.

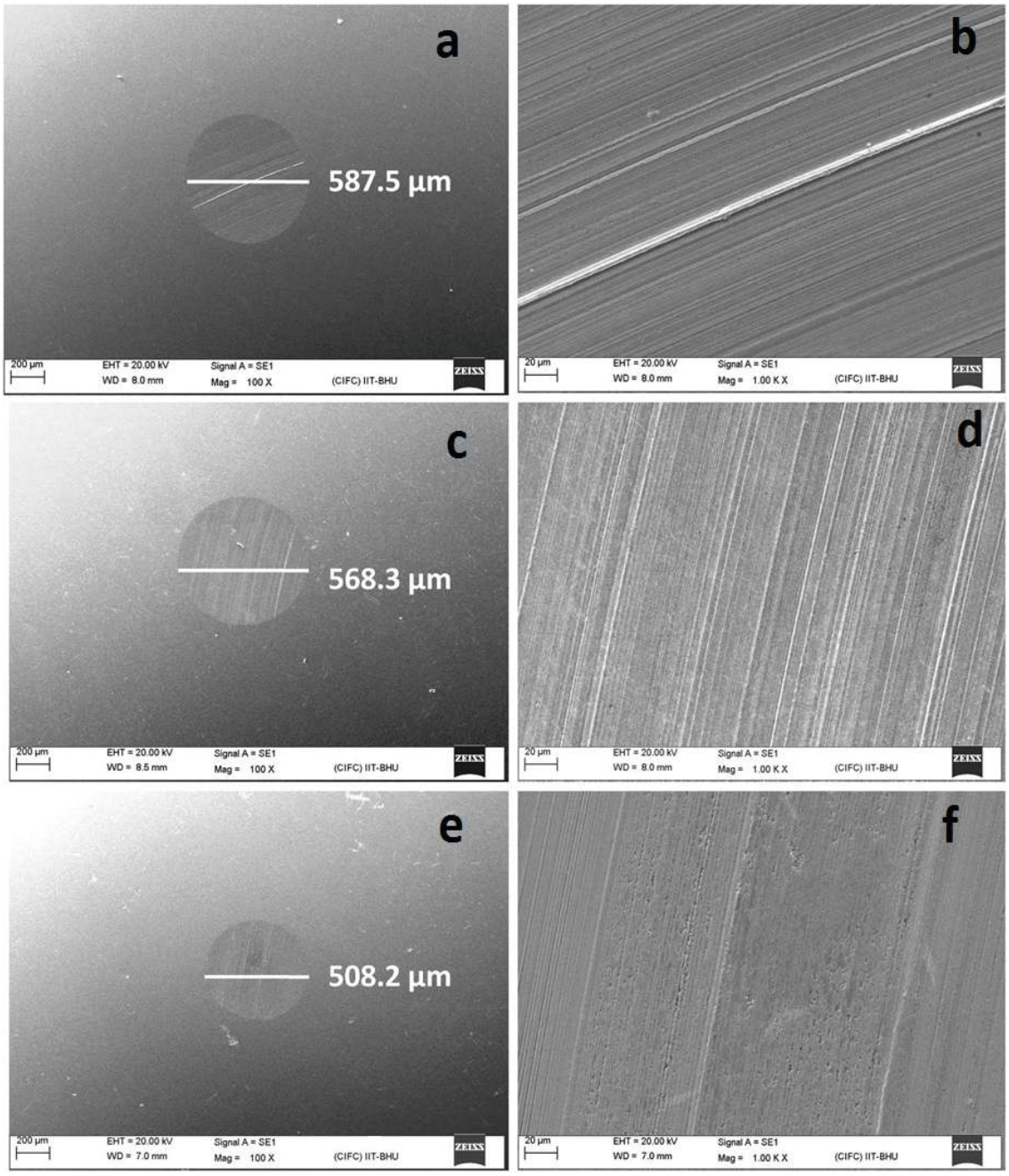

Figure 6.21. SEM images of worn surfaces lubricated at optimum concentrations with (a, b) ECO+0.1%w/v S-CuO ; (c, d) ECO+0.1%w/v CeO_2 and (e, f)) ECO+0.5%w/v PTFE at different magnifications. (load 392N, speed 1200 rpm and time 1h)

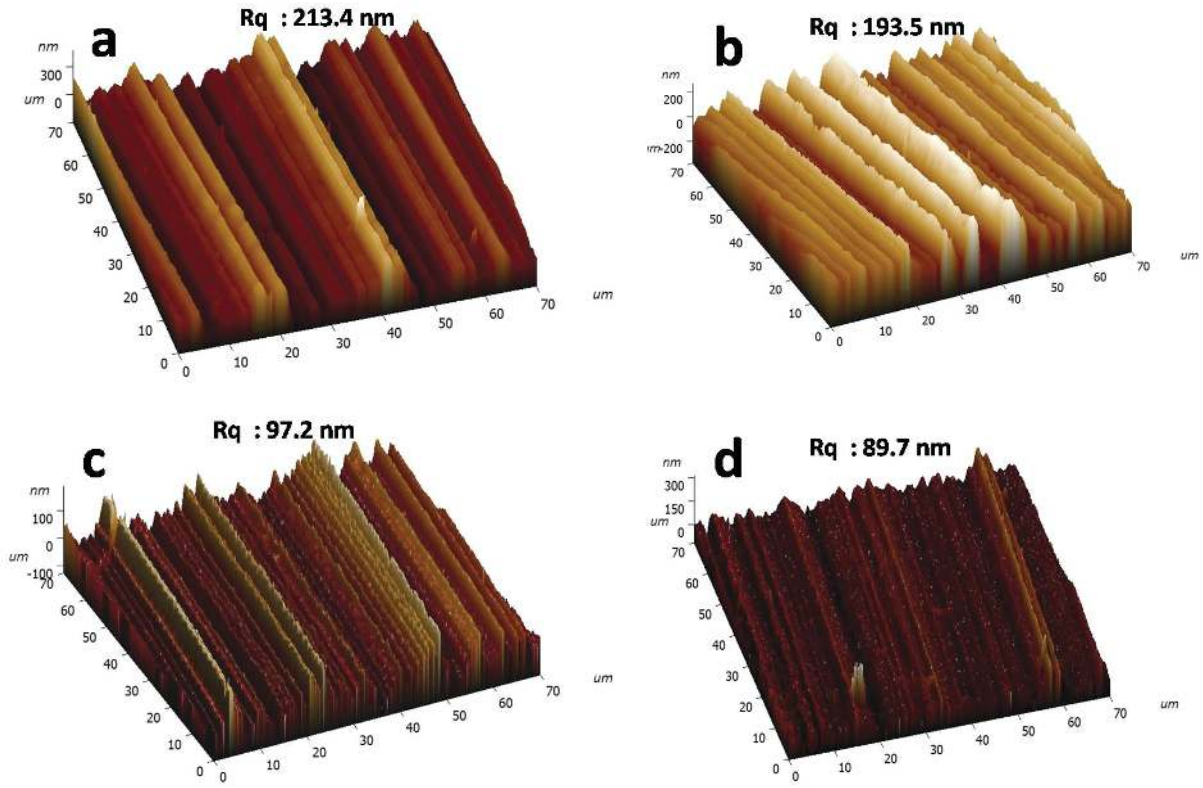

Figure 6.22. SPM roughness images of worn surfaces for (a) ECO, (b) ECO+0.1%w/v S-CuO, (c) ECO+0.1%w/v CeO2 and (d) ECO+0.5%w/v PTFE. (Optimum concentrations) [Tested at load 392N, speed 1200 rpm and time 1h]

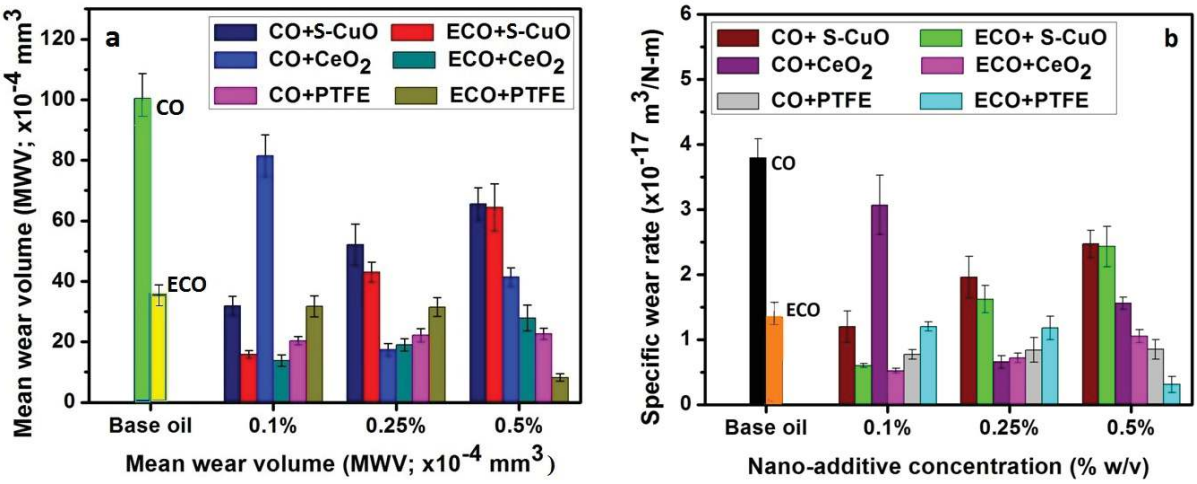

Figure 6.23. Variation of MWV and specific wear rate for all nano-additive concentration in CO and ECO.

Figure 6.23 represents the MWV and specific wear rate for all compositions of nano-additives in ECO. The MWV and specific wear rate at 0.1, 0.1 and 0.5%w/v concentration of S-CuO, CeO_2 and PTFE in ECO exhibits minimum values (Table 6.9). Therefore, these were considered as the optimum concentration. The variation of MWV and specific wear rate follow a similar trend as WSD variation.

6.2.3.2. Antifriction study of modified and unmodified castor oil

Frictional behavior of the CO and ECO based nanolubricants summarized in Table 6.10. The mean COF of ECO (without additive) was reduced by 29.5% as compared to CO. It may be due to good thicker and rapid adsorbed film formation under sliding condition. The presence of polar hydroxyl functional group and formation of the epoxy group after modification enhanced the oil-metal interaction. However, a small amount of nano-additive provides both improved and impaired performance. It was observed that PTFE enhance the friction properties at all the concentration range compare to base ECO (Table 6.10). CeO_2 also show improved mean COF at lower concentration, i.e. 0.1%w/v among all ECO and CeO_2 compositions. On the contrary, S-CuO does not show any improvement at any concentration in ECO. However, as compared to unmodified CO, all the compositions show the improvement either at lower or higher concentration. ECO reveals gradual increase in mean COF along with the concentration of oxide nanoparticles. However, PTFE shows lowest mean COF with the amount of 0.5% in ECO, and it was similar to the CO and PTFE compositions.

Table 6.10. Summary of mean COF and interfacial shear tress for different CO and ECO compositions.

Oil compositions	COF (Avg.)	Interfacial stress (MPa)
CO	0.078	158.5
CO+0.1%S-CuO	0.051	103.7
CO+0.25%S-CuO	0.064	130.1
CO+0.5%S-CuO	0.074	150.5
CO+0.1%CeO_2	0.054	109.2
CO+0.25% CeO_2	0.044	89.9
CO+0.5% CeO_2	0.057	116.7
CO+0.1%PTFE	0.045	90.9
CO+0.25%PTFE	0.036	72.8
CO+0.5%PTFE	0.028	57.9
ECO	0.055	111.8
ECO+0.1%S-CuO	0.053	107.8
ECO+0.25%S-CuO	0.077	156.6
ECO+0.5%S-CuO	0.103	209.5
ECO+0.1% CeO_2	0.041	83.4
ECO+0.25% CeO_2	0.061	124.1
ECO+0.5% CeO_2	0.074	150.5
ECO+0.1%PTFE	0.047	95.6
ECO+0.25%PTFE	0.049	99.7
ECO+0.5%PTFE	0.023	46.8

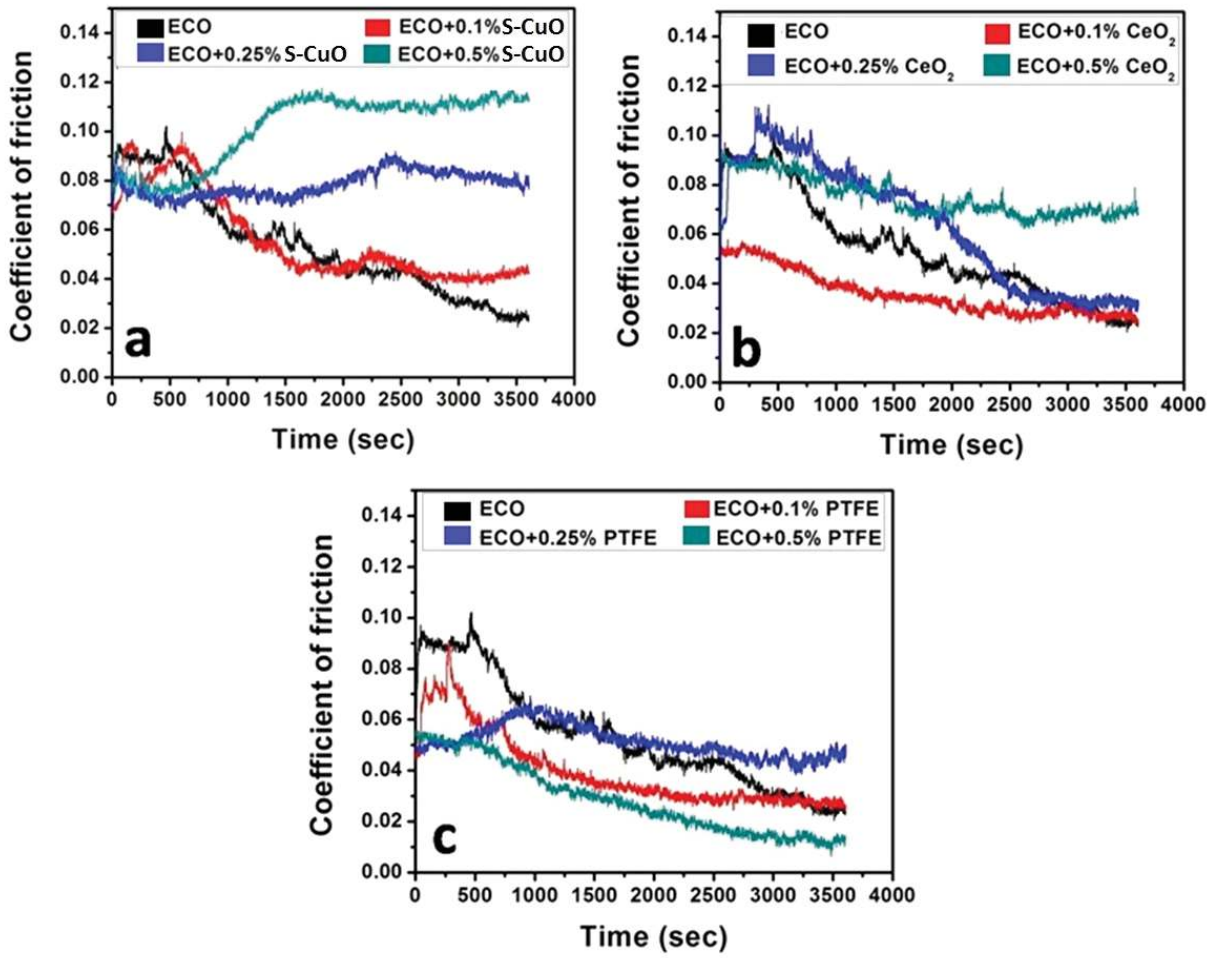

Figure 6.24. Variation in friction coefficient for all ECO compositions with (a) S-CuO, (b) CeO_2 and (c) PTFE. (load 392N, speed 1200 rpm and time 1h)

Figure 6.24 represents the variation of COF throughout the test run. For ECO or lower concentration range of oxide nanoparticles (S-CuO and CeO_2) in ECO, COF continuously reduced up to asymptotic value from start to the end of the test. However, at higher concentration range it shows almost constant or increasing trend (Figure 6.24a and b). On the contrary, PTFE in ECO indicates continuous reduction in COF behavior at all concentrations with lowest at 0.5%w/v (Figure 6.24c). In initial few seconds increment in the COF indicates running-in period and not the formation of sufficient protective film.

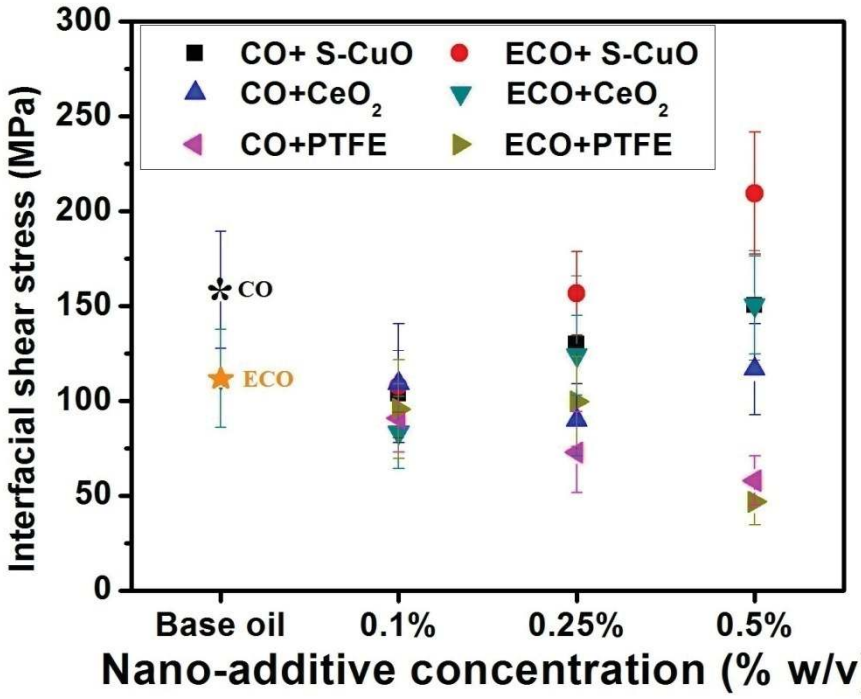

Figure 6.25. Interfacial stress variation for different nanoparticle concentration in CO and ECO.

Figure 6.25 depicts the variation in interfacial shear stress for all ECO and CO compositions. It also shows a similar trend as mean COF variation. PTFE with 0.5%w/v in ECO exhibits lowest interfacial stress among all ECO composition. Lower interfacial stress attributed to better lubrication. On the contrary, S-CuO with 0.5%w/v concentration in ECO shows highest interfacial stress even than base oils CO and ECO. It indicates severe third body abrasion between the mating surfaces. This observation elucidate that S-CuO was not compatible with ECO as a friction modifier. It also observed in most of the cases in the chapter-5 (section 5.3.2.1). The reason may be the irregular shape and relative bigger size than CeO_2 and PTFE. The lowest S-CuO concentration in ECO shows slight improvement in antiwear and antifriction performance. Probably, the increase in viscosity of ECO reflects the

prolonged nanoparticle suspension in achieving the improved tribo-properties. Also, all the nanoparticles with CO shows enhance friction performance.

6.2.3.3. Extreme-pressure study of modified and unmodified castor oil

In EP test, only 0.5% amount of CeO_2 nanoparticles improved the last non-seizure load and weld load capacity as 160 and 200 kgf respectively. However, S-CuO and PTFE show independent behavior in ECO at any concentration. It gives same last non-seizure (126 kgf) and weld load (160 kgf) as the base oil. The similar behavior was also observed for nano-additives in CO with 0.1 to 0.5%w/v concentrations. An important observation is that the modification of the castor oil does not change the extreme pressure properties. The reason for such improvement was similar as discussed in section 6.2.1.3. Under higher sliding speed and contact stress, only the higher amount of the nano-additives provides the threshold particles (even after squeezing action), which stay at the interface and separate the asperities.

6.3. Summary of the chapter

The epoxidation of the biolubricant altered the structure of the fatty acid chain. This change of C=C structure into epoxy group (by forming oxirane ring) enhanced the oil-metal interaction. Therefore, epoxidized oils (without additive) were sufficient to improve the tribo-performance substantially. CeO_2 and PTFE have shown better compatibility than S-CuO nanoparticles. Lower concentration range of nano-additives in oil improved the tribological behavior better than higher amount.